PSU-IRL-SCI-452
Classification Numbers: 1.5, 1.5.1, 1.5.2

Scientific Report 452

An Investigation of Accelerating Mode and Decelerating Mode Constant-Momentum Mass Spectrometry and Their Application to a Residual Gas Analyzer

by

Yee Seung Ng

January 20, 1977

The research reported in this document has been supported by the National Aeronautics and Space Administration under Grant No. NGR 39-009-032.

Submitted by: B R F Kendall
B. R. F. Kendall
Professor of Physics

Approved by: J. S. Nisbet
J. S. Nisbet, Director
Ionosphere Research Laboratory

Ionosphere Research Laboratory

The Pennsylvania State University

University Park, Pennsylvania 16802

TABLE OF CONTENTS

LIST OF FIGURES

ABSTRACT

A theoretical analysis of constant-momentum mass spectrometry is made. A maximum resolving power for the decelerating mode constant-momentum mass spectrometer is shown theoretically to exist for a beam of ions of known energy.

A vacuum system and an electron beam ionization source have been constructed. Supporting electronics for a residual gas analyzer have been built. Experimental investigations of various types of accelerating and decelerating impulsive modes of constant-momentum mass spectrometer as applied to a residual gas analyzer are made. The data indicate that the resolving power for the decelerating mode can be comparable to that of the accelerating mode.

With a reasonable voltage of 200 volts, a short flight path for ions (6.6 cm), compactness, simplicity of operation, high sensitivity and a resolving power of 10, the residual gas analyzer could be used as a nonmagnetic residual gas analyzer in the ionosphere from 250 Km to 80 Km.

CHAPTER I

INTRODUCTION

1.1 Constant-Momentum Mass Spectrometry

The original studies of the constant-momentum mass analyzer (CMMA) were carried out more or less simultaneously by Hipple (1953), M. M. Wolff and W. E. Stephens (1953) and V. B. Fiks (1956). W. M. Brubaker (1958) patented a CMMA consisting of two cylindrical electrostatic energy analyzers (EEA) and a planar impulsive accelerating field. B. R. F. Kendall (1959, 1960) also worked on a CMMA consisting of a planar accelerating impulsive field and a cylindrical EEA. Further developments were made by J. Bracher (1965), I. E. Dayton (1966), and H. M. Luther (1966). All the spectrometers discussed above are of the accelerating type.

A decelerating CMMA was proposed by H. M. Luther and B. R. F. Kendall (1966) and subsequent experimental work has been done by Luther (1970).

1.2 Statement of the Problem

The objectives of this thesis are: (1) the study of accelerating and decelerating modes of the CMMA, and, (2) the development of a compact, high sensitivity residual gas analyzer using the CMMA technique capable of operating even at high pressure (5×10^{-3} Torr). Since the dimensions of the analyzer are much less than the mean free path of the ions even at such a high pressure, the instrument is suitable for residual gas analysis in the region of the ionosphere between 80 and 250 km where the pressure varies from 10^{-3} Torr to 10^{-7} Torr. Measurements of neutral particles in the ionosphere were reviewed by N. W.

Spencer (1971). The sensitivities of almost all of the instruments are 10^{-5} to 10^{-6} amp/Torr. It would be very desirable to get an instrument with high sensitivity but without additional weight due to an extra electron multiplier.

The first step in accomplishing these objectives was the theoretical study of the constant-momentum mass spectrometer with planar geometry in an attempt to optimize its resolving power and sensitivity. The second step was the construction of an electron beam ionization source capable of a reasonably small energy spread in the ionized beam. The third step was the experimental investigation of various types of accelerating and decelerating impulsive modes of the CMMA using the ion source.

CHAPTER II

THEORY OF CONSTANT-MOMENTUM MASS SPECTROMETER

2.1 Basic Theory

When singly charged ions of the same initial energy E_i are traversing a region to which an electric field E(t) of short duration t is applied, ions of different masses gain or lose an identical impulsive momentum P_c, provided the time duration t of the field is less than the time to traverse the region. The impulsive momentum is

$$P_c = \int_t e\, E(t)\, dt \qquad (1)$$

where e is the charge on an ion. The impulsive energy E_c is defined as

$$E_c = \frac{k}{m} P_c^2 \qquad \text{Def. 1}$$

and it is mass dependent. The constant k is equal to .483 in a system of units developed by W. M. Brubaker (1966); time is measured in μ seconds, mass in amu, voltage in volts, energy in eV and distance in cm.

The final energy E_f of the ions after traversing the pulsing region will be

$$E_f = \frac{k}{m} (P_i \pm P_c)^2 \qquad (2)$$

where P_i stands for the initial ion momentum. The positive sign represents an impulsive momentum gain with an accelerating pulse, the negative sign an impulsive momentum loss with a decelerating pulse.

When E_f is expressed in terms of E_i and E_c, one gets

$$E_f = E_i + E_c \pm 2\sqrt{E_i E_c} \qquad (3)$$

which is mass dependent. Thus if an energy analyzer is employed after the pulsing region, ions of different masses can be separated. The above treatment is equivalent to H. M. Luther (1970).

2.2 Effects of the Impulsive Field upon Initial Ion Energy Scatter and Mass Dispersion

Assume a planar pulsing region of length d is used, and a voltage difference V is maintained between the two end plates of that region for a short duration t. Then singly charged ions in the pulsing region will acquire an impulsive momentum.

$$P_c = \frac{e\ V\ t}{d} \tag{4}$$

If the ions enter the planar region at an angle α_i with respect to the axis of the region, then

$$\vec{P}_i = \vec{P}_z + \vec{P}_\rho \tag{5}$$

If $|\vec{P}_z|$ is the magnitude of the initial ion momentum along the axis of the planar region and $|\vec{P}_\rho|$ is the magnitude of the radial initial ion momentum, then

$$|\vec{P}_\rho| = P_\rho = P_i \sin \alpha_i \tag{6}$$

$$|\vec{P}_z| = P_z = P_i \cos \alpha_i \tag{7}$$

Therefore, $E_i = \frac{k}{m} (P_z^2 + P_\rho^2)$ (8)

$$E_f = \frac{k}{m} [(P_z \pm P_c)^2 + P_\rho^2] \tag{9}$$

Substituting equation (6) and equation (7) in equation (9), one gets

$$E_f = \frac{k}{m} (P_i^2 + P_c^2 \pm 2 P_i P_c \cos \alpha_i) \tag{10}$$

Expressed in terms of E_i and E_c, this becomes

$$E_f = E_i + E_c \pm 2\sqrt{E_i E_c} \cos \alpha_i \tag{11}$$

The final ion energy scatter ΔE_f due to an initial ion energy scatter ΔE_i (full width at half height of the mass peak) can be determined from a Taylor expansion

$$\Delta E_f = \frac{\partial E_f}{\partial E_i} \Delta E_i + \frac{1}{2} \frac{\partial E_f}{\partial E_i^2} (\Delta E_i)^2 + \ldots .$$

Using equation (11), one gets to first order in ΔE_i,

$$\Delta E_f (\Delta E_i) = \Delta E_i (1 \pm \sqrt{E_c/E_i} \cos \alpha_i) \tag{12}$$

The positive sign indicates an accelerating pulse, the negative sign a decelerating pulse. As $\alpha_i \to 0$, one gets

$$\Delta E_f (\Delta E_i) = \Delta E_i (1 \pm \sqrt{E_c/E_i}) \tag{13}$$

which parallels Luther (1970).

The difference in final ion energy for different ion masses $(\Delta E_f)_{\Delta m}$ after the impulsive field has been applied can be calculated by using a Taylor expansion of $E_f(m)$ about m.

$$E_f (m + \Delta m) = E_f (m) + \frac{\partial E_f}{\partial m} \Delta m + \ldots . \tag{14}$$

To first order in Δm,

$$\begin{aligned} (\Delta E_f)_{\Delta m} &= E_f(m + \Delta m) - E_f (m) \\ &= \frac{\partial E_f}{\partial m} \Delta m \end{aligned}$$

If one lets

$$C = k\, P_c^{\,2} \tag{15}$$

then

$$E_c = \frac{C}{m} \tag{16}$$

Using equation (11) one gets

$$(\Delta E_f)_{\Delta m} = -\frac{C}{m^2}\left(1 \pm \sqrt{E_i\, m/C}\,\cos\alpha_i\right)\Delta m$$

$$= -\frac{E_c}{m}\left(1 \pm \sqrt{E_i/E_c}\,\cos\alpha_i\right)\Delta m \tag{17}$$

Therefore

$$\frac{m}{\Delta m} = \frac{E_c\left(1 \pm \sqrt{E_i/E_c}\,\cos\alpha_i\right)}{(\Delta E_f)_{\Delta m}} \tag{18}$$

$(\Delta E_{fa})_{\Delta m}$ is defined as the apparent energy spread of the ions at mass m as seen at the analyzer. It is the sum of the energy resolution of the analyzer ε and the final energy spread $\Delta E_f(\Delta E_i)$ due to the initial energy spread ΔE_i (see also Figure 2.1a).

$$(\Delta E_{fa})_{\Delta m} = \varepsilon + \Delta E_f\ (\Delta E_i)$$

From equation (12), one finds

$$(\Delta E_{fa})_{\Delta m} = \varepsilon + \Delta E_i\ \left(1 \pm \sqrt{E_c/E_i}\,\cos\alpha_i\right) \tag{19}$$

If m is just resolvable from m + Δm, then $(\Delta E_f)_{\Delta m}$ is equal to $(\Delta E_{fa})_{\Delta m}$ (see Figure 2.1h).

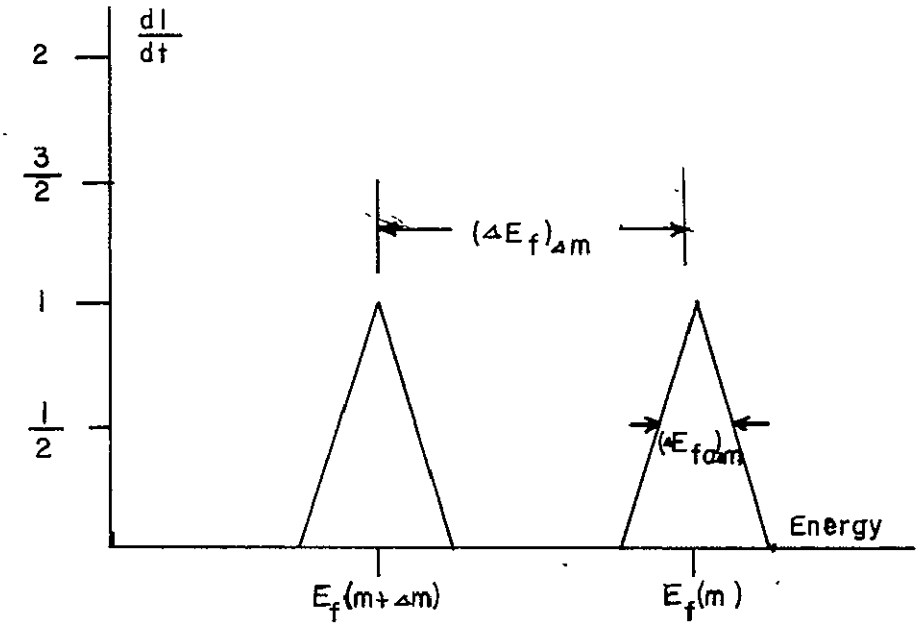

Fig. 2.1.a: Apparent Spectrum of masses m and m+Δm at the Analyzer

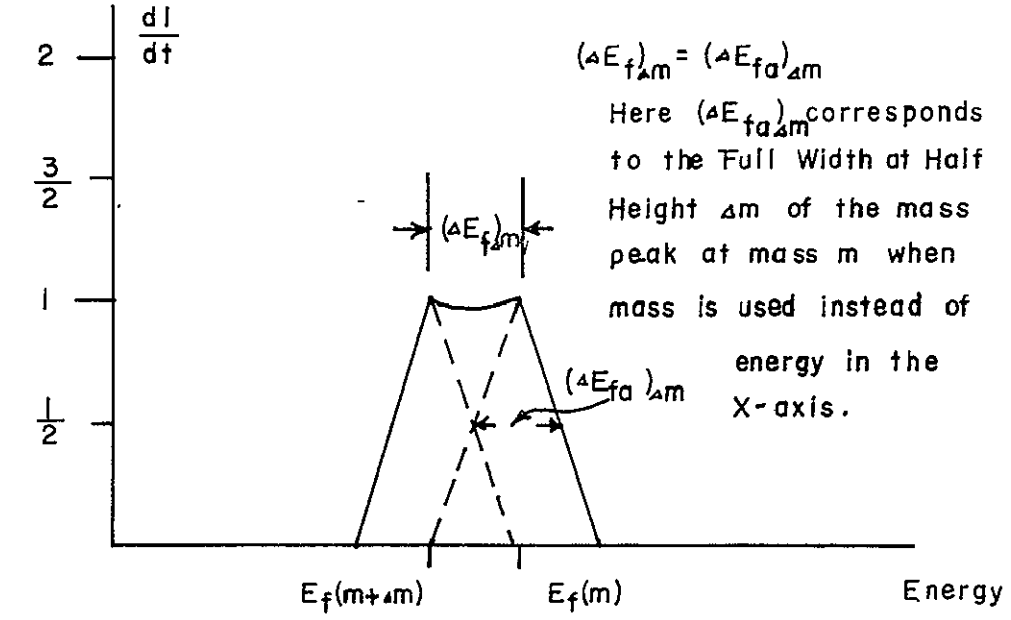

Fig.2.1.b: Apparent Spectrum at the Analyzer when the masses m and m+Δm are just resolvable

2.3 Resolving Power

There are two definitions of resolving power. One is

$$R(m) = \left|\frac{m}{\Delta m}\right| \qquad \text{Def. 2}$$

R(m) is the resolving power at mass m, and Δm is the width of the mass peak in mass units measured at the half-height of the mass peak.

If the ion energy analyzer has an energy resolution of ε, and if $\Delta E_i = 0$, then from equations (18) and (19),

$$R(m) = \left|\frac{m}{\Delta m}\right| = \frac{E_c \left|(1 \pm \sqrt{E_i/E_c} \cos \alpha_i)\right|}{\varepsilon} \qquad (20)$$

If $\Delta E_i \neq 0$, then from equations (18) and (19), the effective resolving power is

$$R(m, \Delta E_i) = \frac{E_c \left|(1 \pm \sqrt{E_i/E_c} \cos \alpha_i)\right|}{\varepsilon + \Delta E_i \left|(1 \pm \sqrt{E_c/E_i} \cos \alpha_i)\right|} \qquad (21)$$

When $\alpha_i = 0$, equation (21) will be the same as equation (77) of Luther (1970).

$$R(m, \Delta E_i) = \frac{E_c \left|(1 \pm \sqrt{E_i/E_c})\right|}{\varepsilon + \Delta E_i \left|(1 \pm \sqrt{E_c/E_i})\right|} \qquad (22)$$

The positive sign represents an accelerating pulse, the negative sign a decelerating pulse.

The other definition of the resolving power is

$$R_0 = |m_0| \qquad \text{Def. 3}$$

Here the resolving power is the maximum mass m_0 such that the mass peak is resolvable from the mass $m_0 + 1$. For $\varepsilon = 0$, we get from equation (22), in an accelerating pulse case,

$$R_0\ (\Delta E_i) = \frac{E_c\ (1 + \sqrt{E_i/E_c}\ )}{\Delta E_i\ (1 + \sqrt{E_c/E_i}\ )}$$

Using equation (16) one gets

$$R_0\ (\Delta E_i) = |m_0| = \frac{C/m_0\ (1 + \sqrt{E_i\ m_0/C}\ )}{\Delta E_i\ (1. + \sqrt{\ C/m_0\ E_i}\ )}$$

$$= \frac{C}{m_0\ \Delta E_i}\ \left(\frac{\sqrt{C}\ + \sqrt{E_i\ m_0}}{\sqrt{m_0\ E_i} + \sqrt{C}}\right)\ \sqrt{m_0\ E_i/C}$$

$$= \frac{1}{\Delta E_i}\ \sqrt{C\ E_i/m_0} \tag{23}$$

Then when equation (15) is used, that is

$$C = k\ P_c^{\ 2} = k\ \left(\frac{e\ V\ t}{d}\right)^2 \tag{24}$$

one gets

$$(m_0)^{3/2} = \frac{1}{\Delta E_i}\ (k\ E_i)^{1/2}\ \left(\frac{e\ V\ t}{d}\right)$$

or

$$R_0\ (\Delta E_i) = |m_0| = (\Delta E_i)^{-2/3}\ (k\ E_i)^{1/3}\ \left(\frac{e\ V\ t}{d}\right)^{2/3} \tag{25}$$

So from equation (25), the resolving power of the accelerating mode $R_0\ (\Delta E_i)$ is proportional to $V^{2/3}\ (\Delta E_i)^{-2/3}\ E_i^{\ 1/3}$.

When $\alpha_i = 0$, it is experimentally convenient to define the measurable resolving power as (see Luther, 1970)

$$R_{exp}\ (m) = \left[\frac{E_c\ |(1 \pm \sqrt{E_i/E_c}\ )|}{\Delta E\ (m)}\right]_{0.5}$$

The subscript 0.5 indicates that the measurement of $\Delta E(m)$ is made at the half height of the mass peak.

2.4 Effect on Resolving Power when the Energy of the Analyzer is Fixed

From equation (16) one knows that when Vt is a constant, $E_c = k/m\ (e\ V\ t/d)^2$ is inversely proportional to m. Thus it follows from equation (22) that $R(m,\Delta E_i)$ will be mass dependent. If we can keep E_c constant irrespective of m, $R(m,\Delta E_i)$ will not be so mass sensitive. This can be achieved if one fixes the energy analyzer's voltage and changes the width of the pulse t. If t is proportional to the voltage output of a ramp function of real time τ, then different masses will gain equal energy at different times τ, will pass through the analyzer at different times, and can be detected. Therefore, in the time scale τ a mass m will pass through at $\tau(m)$, and a mass $m + \Delta m$ will pass through at $\tau(m + \Delta m)$. In a Taylor expansion,

$$\tau(m + \Delta m) = \tau(m) + \frac{\partial \tau}{\partial m} \Delta m + \ldots . \qquad (26)$$

Since t (pulse width) is proporational to τ (time scale), there is a relationship between t and τ, such as

$$t = g + f\tau \qquad (27)$$

where g and f are constants.

Therefore, $\tau(m + \Delta m) - \tau(m) = \Delta\tau_m$

$$= \frac{\partial \tau}{\partial m} \Delta m \qquad (28)$$

to first order in Δm.

$$\text{And } \Delta\tau_m = \frac{\partial \tau}{\partial t} \frac{\partial t}{\partial m} \Delta m \qquad (29)$$

From equation (16)

$$t = \left(\frac{m\ E_c}{k}\right)^{1/2} \left(\frac{d}{eV}\right) \qquad (30)$$

If the energy analyzer is fixed at E_f and E_c is a constant, then from equation (30) one gets

$$t = m^{1/2} C_1 \tag{31}$$

where

$$C_1 = \left(\frac{E_c}{k}\right)^{1/2} \left(\frac{d}{eV}\right) \tag{32}$$

Using equations (27) and (31) in equation (29), one gets

$$\Delta\tau_m = \frac{1}{2f} C_1 m^{-1/2} \Delta m \tag{33}$$

$$= \frac{t}{2f} \frac{\Delta m}{m} \tag{34}$$

Therefore,

$$\left|\frac{m}{\Delta m}\right| = \left|\frac{t}{2f\Delta\tau_m}\right| = \left|\frac{t}{2\Delta t}\right| \tag{35}$$

For a certain mass m, the difference in final energy as t changes can be found by using a Taylor expansion of $E_f(t)$ about t:

$$E_f\ (t + \Delta t) + E_f(t) + \frac{\partial E_f}{\partial E_c} \frac{\partial E_c}{\partial t} \Delta t + \ldots . \tag{36}$$

then

$$\Delta E_f = E_f\ (t + \Delta t) - E_f(t)$$

When equation (11) is used one gets to first order in Δt,

$$\Delta E_f(t) = \frac{2E_c}{t} \Delta t\ (1 \pm \sqrt{E_i/E_c}\ \cos \alpha_i) \tag{37}$$

Here Δt is the difference in pulse width when E_f changes from $E_f(t)$ to $E_f\ (t + \Delta t)$.

If one lets

$$E_c = \frac{b}{m} t^2 \tag{38}$$

where

$$b = k\left(\frac{V}{d}\right)^2 \tag{39}$$

and uses equations (38) and (39) in equation (11), one gets

$$E_f = E_i + \frac{b}{m} t^2 \pm 2 t \sqrt{E_i \frac{b}{m}} \cos \alpha_i \tag{40}$$

One gets

$$t(m, E_i) = \sqrt{m/b} \left(\mp \cos \alpha_i \sqrt{E_i} \pm \sqrt{E_f - E_i \sin^2 \alpha_i}\right) \tag{41}$$

with the condition that $E_f \geq E_i \sin^2 \alpha_i$.

Therefore from equation (38), one gets

$$E_c = \left(\mp \cos \alpha_i \sqrt{E_i} \pm \sqrt{E_f - E_i \sin^2 \alpha_i}\right)^2 \tag{42}$$

Then from equation (37) one gets a relationship between Δt and $\Delta E_f(t)$

$$\Delta t = \frac{t}{2} \frac{\Delta E_f(t)}{E_c} \cdot \frac{1}{(1 \pm \sqrt{E_i/E_c} \cos \alpha_i)} \tag{43}$$

If $\Delta E_f(t)$ is the apparent energy spread of the ions of mass m which will just be energetically enough to pass through the analyzer when the pulse width is t, then $\Delta E_f(t) = (\Delta E_{fa})_{\Delta m}$ and from equation (19), one gets

$$\Delta E_f(t) = \varepsilon + \Delta E_i \left(1 \pm \sqrt{E_c/E_i} \cos \alpha_i\right) \tag{44}$$

Therefore Δt can be written as

$$\Delta t = \frac{t}{2} \frac{\Delta E_i \left(1 \pm \sqrt{E_c/E_i} \cos \alpha_i\right) + \varepsilon}{E_c \left(1 \pm \sqrt{E_i/E_c} \cos \alpha_i\right)} \tag{45}$$

and $R(m,\Delta E_i) = \left|\frac{m}{\Delta m}\right| = \left|\frac{t}{2\Delta t}\right|$ will give

$$R(m,\Delta E_i) = \frac{\left|E_c\ (1 \pm \sqrt{E_i/E_c}\ \cos\ \alpha_i)\right|}{\varepsilon + \Delta E_i\ \left|(1 \pm \sqrt{E_c/E_i}\ \cos\ \alpha_i)\right|}$$

which is the same as equation (21).

If one lets

$$R_1(m,\Delta E_i) \doteq \frac{\left|E_c\ (1 \pm \sqrt{E_i/E_c}\ \cos\ \alpha_i)\right|}{\varepsilon} \tag{46}$$

then

$$R(m,\Delta E_i) = \frac{R_1}{1 + \dfrac{R_1\ \Delta E_i\ \left|(1 \pm \sqrt{E_c/E_i}\ \cos\ \alpha_i)\right|}{\left|E_c\ (1 \pm \sqrt{E_i/E_c}\ \cos\ \alpha_i)\right|}} \tag{47}$$

When equation (42) is used one gets

$$R_1(m,\Delta E_i)$$

$$= \frac{1}{\varepsilon}\ \left|(E_f - E_i\ \sin^2\ \alpha_i - \sqrt{E_i}\ \cos\ \alpha_i\ \sqrt{E_f - E_i\ \sin^2\ \alpha_i}\ )\right| \tag{48}$$

If $\alpha_i = 0$, equation (48) becomes

$$R_1(m,E_i) = \frac{1}{\varepsilon}\ \left|(E_f - \sqrt{E_i\ E_f}\ )\right| \tag{49}$$

Then $R_1(m,\Delta E_i)$ is equivalent to equation (107) of Luther (1970).

When $\alpha_i = 0$, $R(m, \Delta E_i)$ from equation (47) will become

$$R(m, \Delta E_i) = \frac{R_1}{1 + \dfrac{R_1\ \Delta E_i\ \left|(1 \pm \sqrt{E_c/E_i}\ )\right|}{\left|E_c\ (1 \pm \sqrt{E_i/E_c}\ )\right|}} \tag{50}$$

From equation (42), one gets

$$E_c = (\pm \sqrt{E_f} \mp \sqrt{E_i})^2 \tag{51}$$

One then can express $R(m,\Delta E_i)$ in terms of E_i, E_f, $R_1(m)$, and ΔE_i. Since all of these will be determined by the instrument alone, $R(m,\Delta E_i)$ will be determined by the instrument alone.

$$R(m,\Delta E_i) = \frac{R_1}{1 + \dfrac{R_1 \, \Delta E_i \, | \sqrt{E_f} \, |}{|(\pm \sqrt{E_i \, E_f}) \, (\pm \sqrt{E_f} \mp \sqrt{E_i})|}} \tag{52}$$

Let

$$G = \frac{E_i}{E_f} \tag{53}$$

then in the accelerating pulse case, one gets

$$R(m,\Delta E_i) = \frac{R_1}{1 + \dfrac{R_1 \, \Delta E_i \, | \sqrt{E_f} \, |}{|\sqrt{E_i \, E_f} \, (\sqrt{E_f} - \sqrt{E_i})|}}$$

$$= \frac{R_1}{1 + \dfrac{R_1 \, \Delta E_i}{|\sqrt{E_i \, E_f} \, (1 - \sqrt{G})|}} \tag{54}$$

and this is the same as equation (109) of Luther (1970).

In the decelerating pulse case one gets

$$R(m,\Delta E_i) = \frac{R_1}{1 + \dfrac{R_1 \, \Delta E_i}{| - E_i + \sqrt{E_i \, E_f} \, |}} \tag{55}$$

which has about the same form as equation (54). That is, if $R(m,\Delta E_i)$ is expressed in terms of G, one will get,

$$R(m,\Delta E_i) = \frac{R_1}{1 + \frac{R_1 \cdot \Delta E_i}{\left|\sqrt{E_i\ E_f}\ (-\sqrt{G} + 1)\right|}} \tag{56}$$

2.5 Effect on Resolving Power when the Ions Going into the Pulsing Region Have a Finite Angular Spread

If the ion beam entering the pulsing region at an angle α_i with respect to the region's axis has an angular spread of $\Delta\alpha_i$ about the ion beam axis, one can find the resolving power by finding $m/\Delta m$, where Δm is expressed in terms of t, Δt, E_i, ΔE_i, α_i, and $\Delta\alpha_i$.

From equation (42), one gets

$$E_c = \left(\pm \sqrt{E_f - E_i \sin^2 \alpha_i} \mp \cos \alpha_i \sqrt{E_i}\ \right)^2 = \frac{bt^2}{m}$$

Therefore,

$$m = \frac{bt^2}{\left(\pm \sqrt{E_f - E_i \sin^2 \alpha_i} \mp \sqrt{E_i} \cos \alpha_i\right)^2} \tag{57}$$

Using a Taylor expansion of m about t, E_i, and α_i, one gets

$$m(t + \Delta t,\ E_i + \Delta E_i,\ \alpha_i + \Delta\alpha_i)$$

$$= m(t,\ E_i,\ \alpha_i) + \left(\frac{\partial m}{\partial t}\Delta t + \frac{\partial m}{\partial E_i}\Delta E_i + \frac{\partial m}{\partial \alpha_i}\Delta\alpha_i\right) \tag{58}$$

Therefore, $\Delta m(t,\ E_i,\ \alpha_i)$

$$= m(t + \Delta t,\ E_i + \Delta E_i,\ \alpha_i + \Delta\alpha_i) - m(t,\ E_i,\ \alpha_i)$$

Using equation (57) one gets

$$\Delta m(t, E_i, \alpha_i)$$

$$= E_c^{-1} \left\{ (2bt)\ \Delta t + \frac{2\ bt^2}{\sqrt{E_c}} \left[\pm \frac{\cos \alpha_i}{2\sqrt{E_i}} \mp \frac{1}{2} \frac{\sin^2 \alpha_i}{\sqrt{E_f - E_i \sin^2 \alpha_i}} \right] \Delta E_i \right.$$

$$\left. - \frac{2\ bt^2}{\sqrt{E_c}} \left[\pm \sqrt{E_i} \sin \alpha_i \mp \frac{E_i \cos \alpha_i \sin \alpha_i}{\sqrt{E_f - E_i \sin^2 \alpha_i}} \right] \Delta \alpha_i \right\} \tag{59}$$

to first order in Δt, ΔE_i, and $\Delta \alpha_i$.

Since $E_c = \frac{bt^2}{m}$, one gets

$$R_m(t, E_i, \alpha_i) = \left| \frac{m(t, E_i, \alpha_i)}{\Delta m(t, E_i, \alpha_i)} \right|$$

$$= \left| \frac{1}{\frac{2}{t} \Delta t + A\ \Delta E_i + B\ \Delta \alpha_i} \right| \tag{60}$$

where

$$A = \left| \frac{1}{\sqrt{E_c}} \left[\pm \frac{\cos \alpha_i}{\sqrt{E_i}} \mp \frac{\sin^2 \alpha_i}{\sqrt{E_f - E_i \sin^2 \alpha_i}} \right] \right| \tag{61}$$

$$B = \left| \frac{2}{\sqrt{E_c}} \left[\pm \frac{E_i \cos \alpha_i \sin \alpha_i}{\sqrt{E_f - E_i \sin^2 \alpha_i}} \mp \sqrt{E_i} \sin \alpha_i \right] \right| \tag{62}$$

If $R_1(m) = \left| t/2\Delta t \right|$ is due to the ε resolution of the analyzer as given in equation (48), then

$$R_m(t, E_i, \alpha_i)$$

$$= \frac{R_1(m)}{1 + R_1(m)\ [A\ \Delta E_i + B\ \Delta\alpha_i]} \tag{63}$$

If $\alpha_i = 0$, B will be zero and the resolution $R_m(t, E_i, \alpha_i)$ is insensitive to the angular spread $\Delta\alpha_i$ of the ion beam.

2.6 Optimization of Resolving Power in the Decelerating Mode

From equation (22) one gets for the decelerating mode

$$R_d(m, \Delta E_i) = \frac{E_c\ |1 - \sqrt{E_i/E_c}\ |}{\varepsilon + \Delta E_i\ |(1 - \sqrt{E_c/E_i}\ )|}$$

However, E_i must be greater than E_c for the ions to traverse the pulsing region without being pushed backward.

$$\text{Let} \quad H = \frac{E_i}{E_c} \tag{64}$$

therefore $H > 1$,

and

$$R_d(m, \Delta E_i) = \frac{E_i\ |1 - \sqrt{H}\ |}{H(\varepsilon + \Delta E_i\ |(1 - \sqrt{1/H}\ )|)}$$

or

$$= \frac{E_i\ |1 - \sqrt{H}\ |}{H(\varepsilon + \Delta E_i\ (1 - \sqrt{1/H}\ ))} \tag{65}$$

Then for a certain E_i one can find a value of E_c such that $R_d(m, \Delta E_i)$ is a maximum at that E_i.

Taking the derivative of equation (65) with respect to H and noting that $|1 - \sqrt{H}\ | = \sqrt{H} - 1$, one gets

$$\frac{dR_d}{dH} = \frac{1}{2}\sqrt{H}\,(\varepsilon + \Delta E_i) - (\varepsilon + \Delta E_i) + \frac{\Delta E_i}{2\sqrt{H}} \tag{66}$$

Setting $dR_d/dH = 0$, one gets

$$H(\varepsilon + \Delta E_i) - 2\sqrt{H}\,(\Delta E_i + \varepsilon) + \Delta E_i = 0 \tag{67}$$

Then $$\sqrt{H} = 1 \pm \sqrt{1 - \left(\frac{\Delta E_i}{\varepsilon + \Delta E_i}\right)}$$

$$= 1 \pm \sqrt{\frac{\varepsilon}{\varepsilon + \Delta E_i}} \tag{68}$$

Since $H > 1$, therefore, for maximum resolution

$$\sqrt{H}_{max,R} = 1 + \sqrt{\frac{\varepsilon}{\varepsilon + \Delta E_i}} \tag{69}$$

From equation (69) one gets for a certain E_i

$$(\sqrt{E_c})_{max,R} = \frac{\sqrt{E_i}}{1 + \sqrt{\frac{\varepsilon}{\varepsilon + \Delta E_i}}}$$

or

$$(E_c)_{max,R} = \frac{E_i}{\left(1 + \sqrt{\frac{\varepsilon}{\varepsilon + \Delta E_i}}\right)^2} \tag{70}$$

At this value R_d is a maximum. One also notices from equation (69) that $(\sqrt{H})_{max,R}$ depends only on ε and ΔE_i, thus from equation (65) one gets an $R_d(m, \Delta E_i)_{max,R}$

$$R_d(m, \Delta E_i)_{max,R} = \frac{E_i\sqrt{\left(\frac{\varepsilon}{\varepsilon + \Delta E_i}\right)}}{\varepsilon\left(1 + \sqrt{\frac{\varepsilon}{\varepsilon + \Delta E_i}}\right)^2 + \Delta E_i\left(1 + \sqrt{\frac{\varepsilon}{\varepsilon + \Delta E_i}}\right)\sqrt{\frac{\varepsilon}{\varepsilon + \Delta E_i}}} \tag{71}$$

therefore, $R_d(m, \Delta E_i)_{max}$ is proportional to E_i as in Figure 2.2.

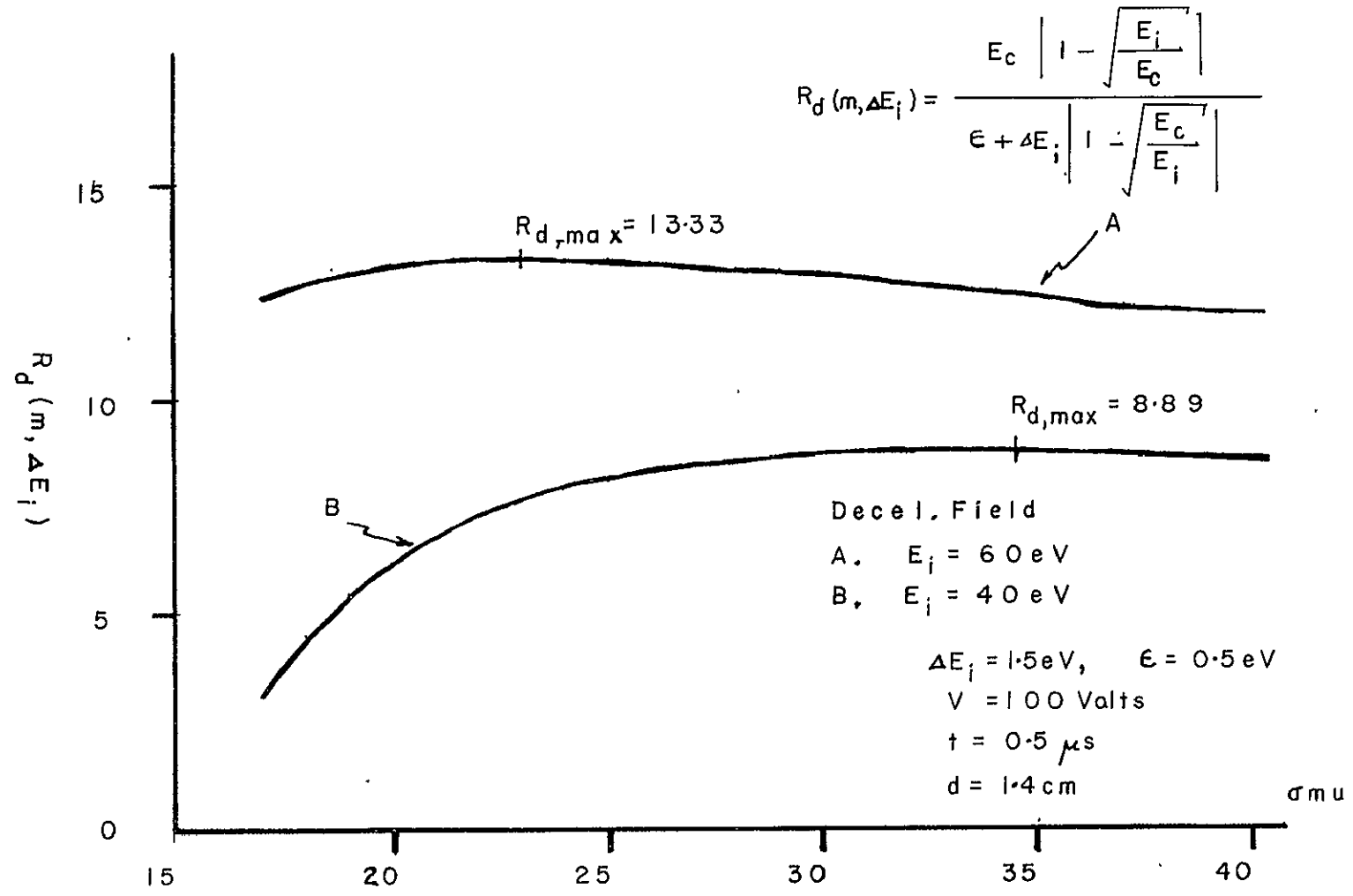

Fig. 2.2: Resolving Power for the Decelerating Field C M M A

Moreover from Section (2.4) one finds that if E_c is fixed, $R_d(m, \Delta E_i)$ will be mass insensitive. One can fix E_c for a certain E_i in order to get $R_d(m, \Delta E_i)_{max}$ for all masses. This can be achieved if the final energy of the analyzer is fixed at $(E_f)_{max,R}$. From equation (11), when $\alpha_i = 0$, one gets

$$E_f = E_i + E_c - 2\sqrt{E_i E_c}$$

for the decelerating mode.

When one uses equation (70) one gets

$$(E_f)_{max,R} = E_i \left[1 + \frac{1}{\left[1 + \sqrt{\frac{\varepsilon}{\varepsilon + \Delta E_i}} \right]^2} - \frac{2}{\left[1 + \frac{\varepsilon}{\varepsilon + \Delta E_i} \right]} \right] \tag{72}$$

which can be reduced to

$$(E_f)_{max,R} = E_i \left[\frac{\frac{\varepsilon}{\varepsilon + \Delta E_i}}{\left[1 + \sqrt{\frac{\varepsilon}{\varepsilon + \Delta E_i}} \right]^2} \right] \tag{73}$$

2.7 Sensitivity

According to the American Vacuum Standard (1972), the sensitivity for a mass analyzer is defined as the change in current output divided by the change in partial pressure of the gas causing the change. The units of sensitivity are usually Amperes per Torr. This parameter for different modes of operations of the constant momentum mass analyzer will be investigated in this report.

2.8 Summary

A few conclusions can be drawn from the previous analysis:

(1) From equation (12) one finds that the planar accelerating field enhances the initial ion energy spread and the planar

decelerating field decreases the initial ion energy spread. The impulsive momentum gain or loss of an ion traversing a planar impulsive field is independent of initial energy E_i and position of the ions within the field region. Both of these conclusions were also reached by Luther (1970).

(2) From equation (21), $R(m, \Delta E_i)$ for both accelerating and decelerating cases will improve if the initial ion energy spread ΔE_i is smaller. Also from the analysis in Section 2.5 the resolving power for both cases will be insensitive to initial angular spread $\Delta\alpha_i$, provided the initial angle that the ion beam makes with the planar axis (α_i) is zero.

(3) From the analysis in Section 2.4 one finds that if E_c is constant, then $R(m, \Delta E_i)$ will be mass insensitive. Also as E_c is set to a larger value, the resolving power would increase; provided ΔE_i and ε remain constant. Both of these were also pointed out by Luther (1970).

(4) For the accelerating mode from Figure 2.3, equation (22) and equation (25), one can conclude that the resolving power will increase as initial energy E_i increases, provided ΔE_i and ε are constants.

(5) For the decelerating mode, from Section 2.6 one finds that for a given E_i there exists an E_c that will give a maximum resolving power $R_d(m, \Delta E_i)_{max,R}$. Therefore if one fixes the analyzer voltage at $(E_f)_{max,R}$ [as in equation (73)] for a given E_i, one can get a maximum resolving power $R_d(m, \Delta E_i)_{max,R}$ as given in equation (71).

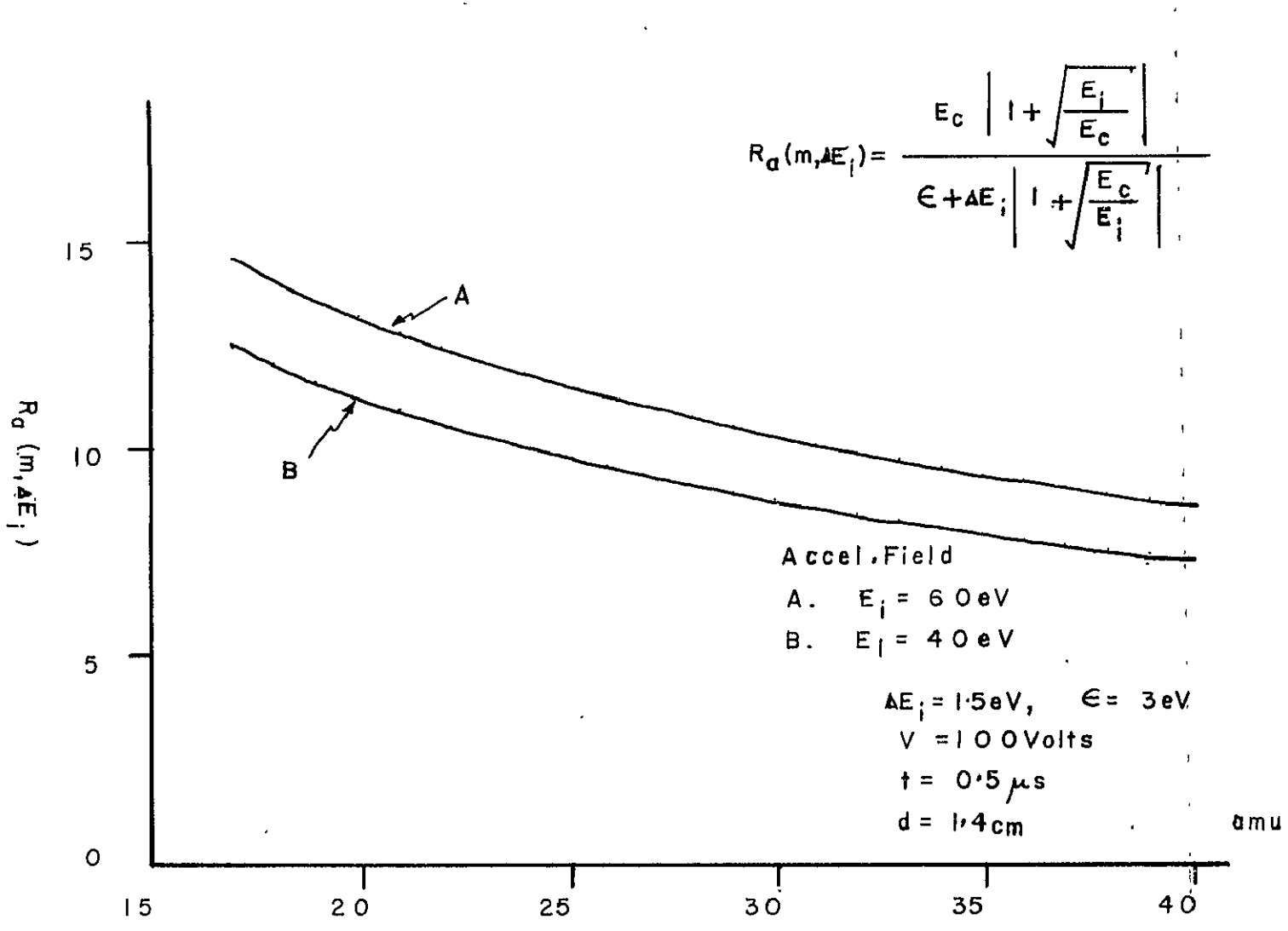

Fig. 2.3: Resolving Power for the Accelerating Field C M M A

(6) As equation (71) and Figure 2.2 show, $R_d(m, \Delta E_i)_{max,R}$ for the decelerating mode will be proportional to E_i. Moreover, the resolving power is very sensitive to the energy resolution of the analyzer ε.

Therefore, one must get ε and ΔE_i as small as possible in order to get the maximum resolving power. It will also help if $\alpha_i = 0$ and E_i is large. In the decelerating case one can get a maximum resolving power if the above condition (5) is satisfied. One also notices from Figure 2.2 and Figure 2.3 that under similar conditions, the resolving power for the decelerating mode is less mass sensitive than that of the accelerating mode even if E_c is not kept constant.

CHAPTER III

BASIC EXPERIMENTAL SET UP

3.1 Vacuum System

The present system is a modification of the one introduced by B. R. F. Kendall and D. R. David (1968). The schematic diagram is drawn in Figure 3.1 using the symbols defined by the American Vacuum Society Standard (1972).

The vacuum system has a gas inlet system and two mechanical forepumps. Mechanical pump 1 is used for the rapid pump-down of the vacuum chamber and, if necessary, evacuation of the gas inlet system. Mechanical pump 2 pumps through a zeolite trap to the vacuum chamber. Liquid nitrogen is used in the zeolite trap to pump the vacuum chamber to a pressure of approximately 10^{-6} Torr. After the zeolite trap is cold, low pressure can be maintained in the vacuum chamber with both pumps off. Thus mechanical vibration due to pumps can be eliminated.

Gases may be injected into the gas inlet system and leaked to the vacuum chamber through the calibrated leak valve.

3.2 Ion Source

In order to make a residual gas analyzer an electron beam ionization source capable of a reasonably small energy spread ΔE_i in the ionized beam is needed. A cross-section of the ion source is shown in Figure 3.2. It was constructed with an ion optics kit developed by B. R. F. Kendall and H. M. Luther (1966). Thoriated tungsten is used as the filament. Since its work function is lower than tungsten, it requires less current to yield an equivalent emission (K. R. Spangenberg, 1957). Repeller 1 and electron lens 1 are used to extract the electrons.

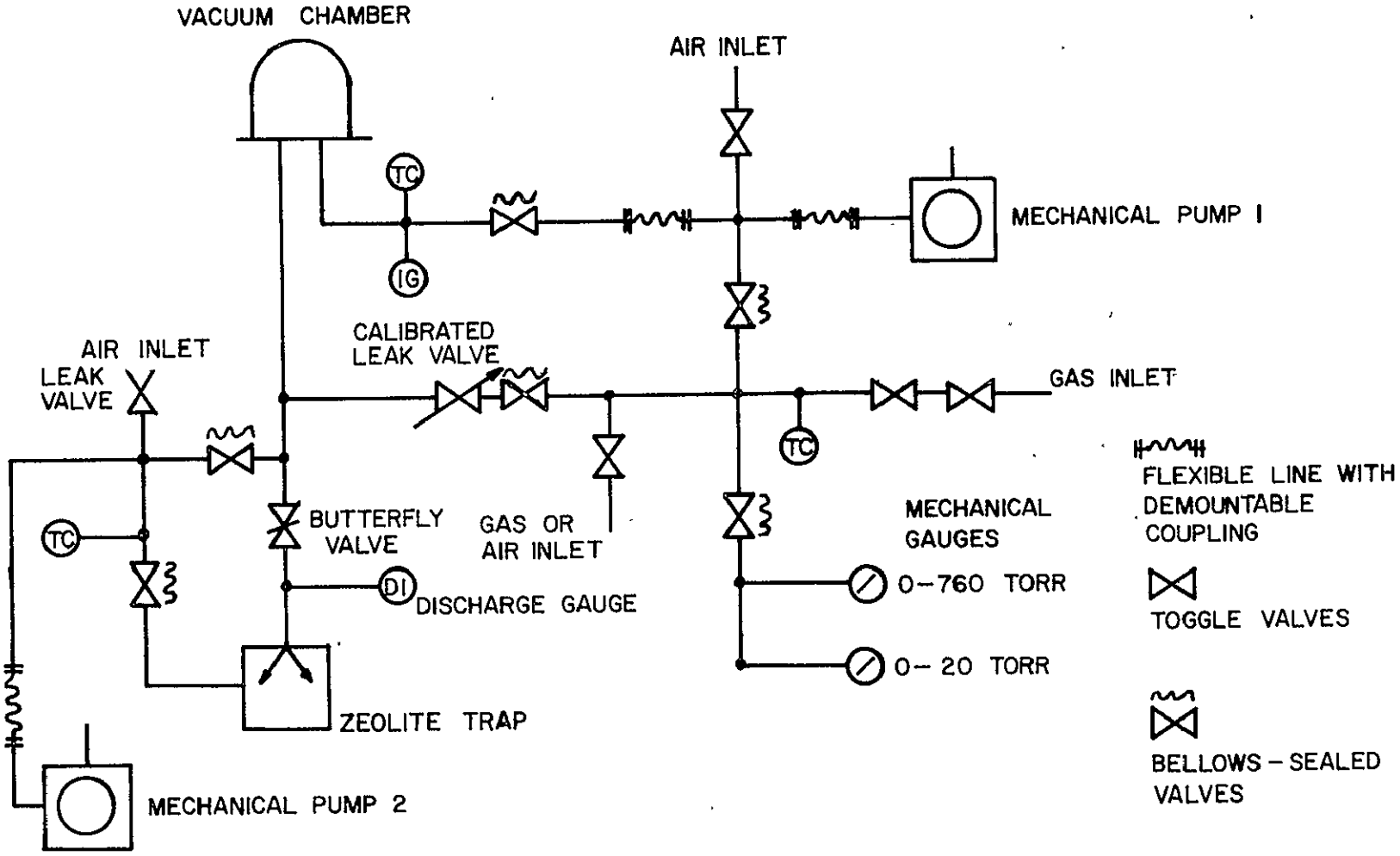

FIG. 3.1 SCHEMATIC DIAGRAM FOR THE VACUUM SYSTEM

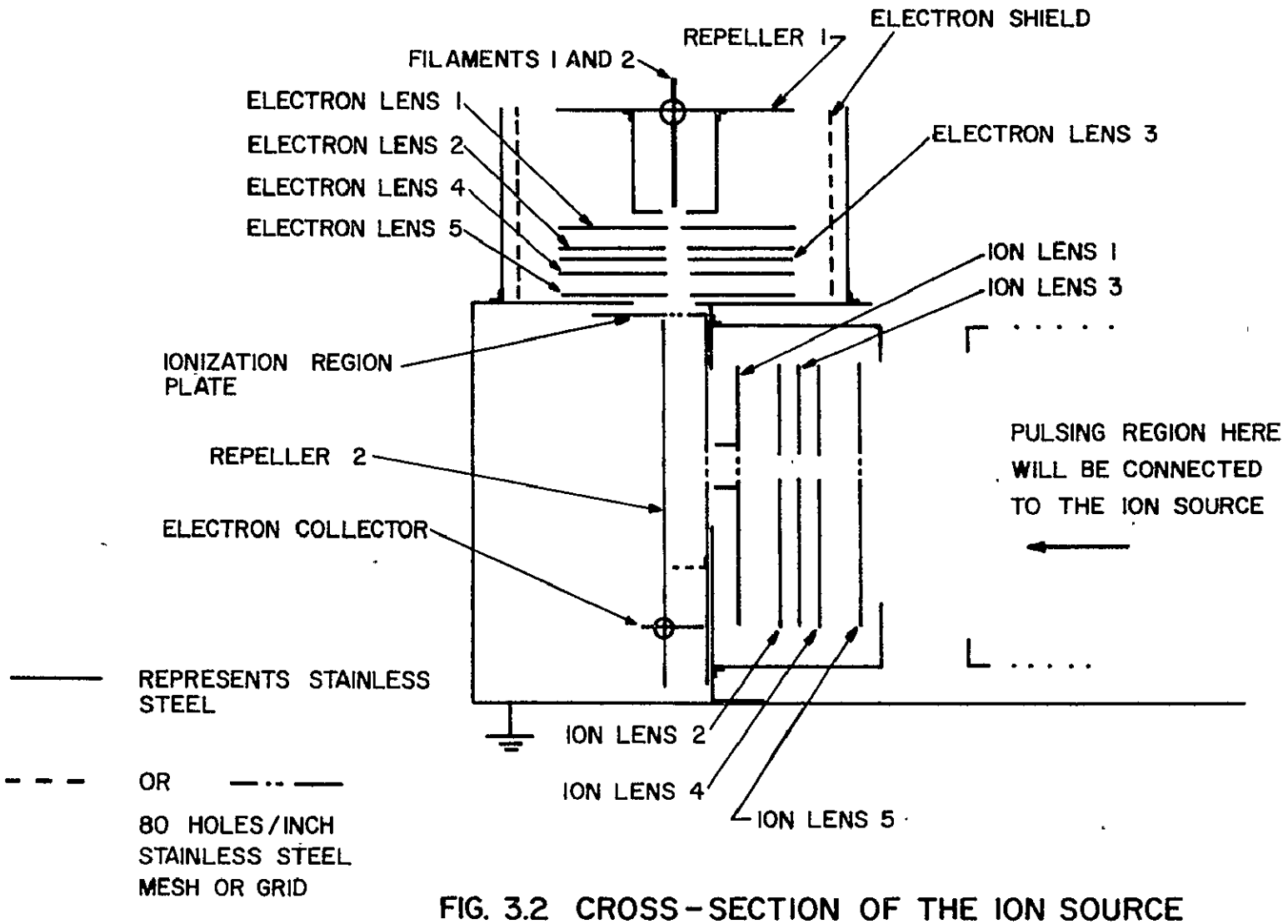

FIG. 3.2 CROSS-SECTION OF THE ION SOURCE

Before going into the ionization region the electron beam is focused into a parallel beam by the einzel lens (O. Klemperer, 1971 and K. Kanaya, 1966) consisting of electron lens 2, electron lens 3 and electron lens 4. Electron lens 5 is used to maintain a field-free region between electron lens 4 and the ionization region plate by minimizing the effects of the grounded supports which are close to them.

One can limit ΔE_i to a very small value by maintaining a small D.C. potential between the repeller 2 plate and the ionization region plate. The efficiency of ionization of gases can be maximized by adjusting the potential difference between the ionization region and the D.C. bias of the filament. For the gases of interest it will be approximately 80 eV (S. Dushman, 1949).

The ion beam will be extracted from the ionization region by ion lens 1 and refocused into a parallel beam by another einzel lens consisting of ion lens 2, ion lens 3 and ion lens 4. If $\alpha_i = 0$, resolving power will be maximized. If $\Delta\alpha_i$ is very small sensitivity can also be maximized. Ion lens 5 isolates the einzel lens from the pulsing region to the right of the ion source.

The design of this ion source gives a large flexibility in the choice of E_i and ΔE_i while maximizing the efficiency of ionization. The supporting electronics for the ion source are shown in Figure 3.3.

All materials used in the ion source are stainless steel and the connecting wires inside the vacuum are either Teflon-coated or polyamide-coated.

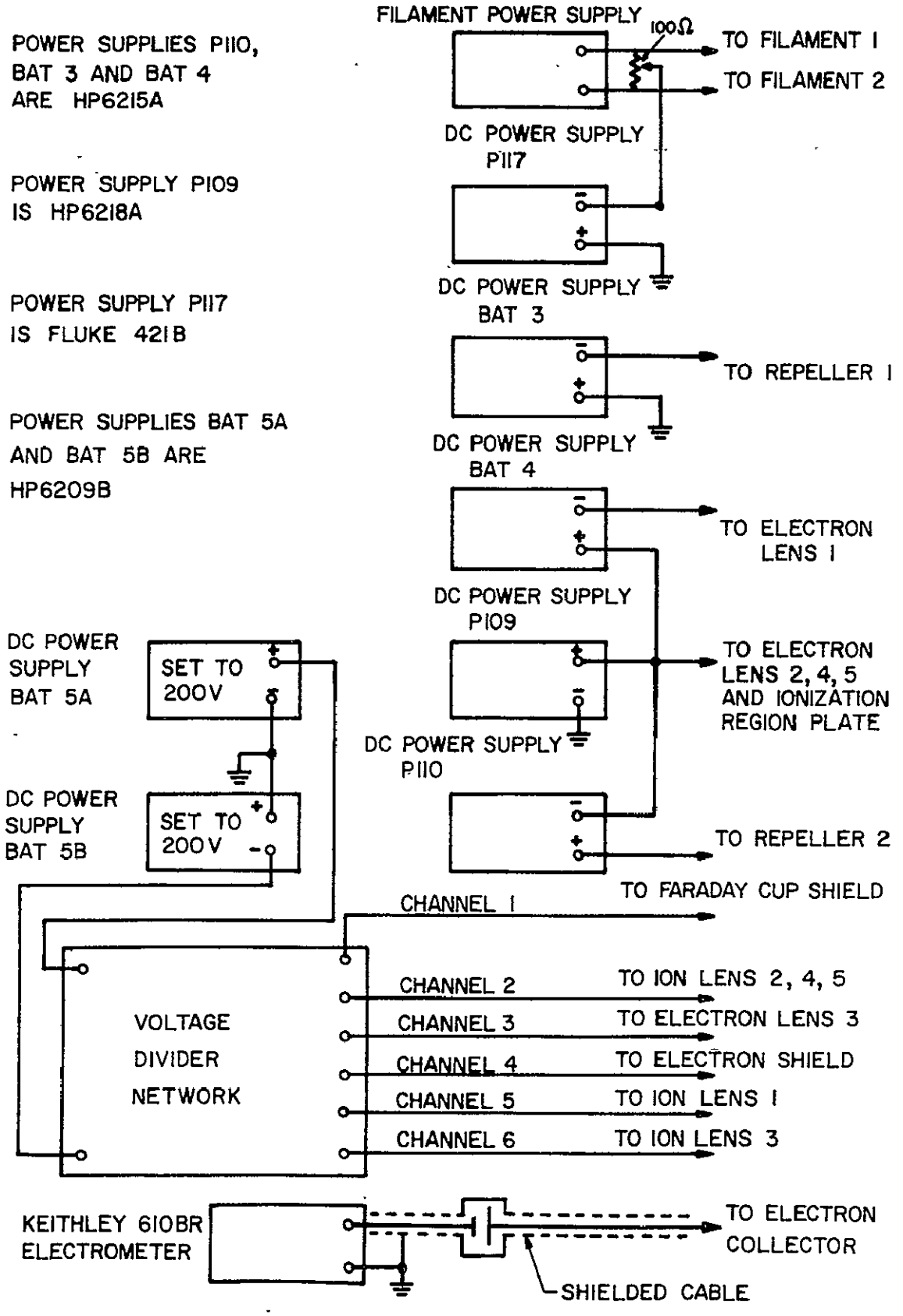

FIG. 3.3. SUPPORTING ELECTRONICS FOR THE ION SOURCE

3.3 Some Basic Supporting Electronics

3.3.1 Twin-Output Function Generator

From section (2.4) one finds that if the impulsive energy E_c can be held constant irrespective of m, $R(m,\Delta E_i)$ will not be so mass sensitive. This can be achieved by fixing the energy analyzer's voltage and changing the width of the pulse t. A Velonex Model V-1589 pulse generator generates a pulse whose width is proportional to a voltage input to it. I have constructed a function generator with twin outputs (Figures 3.4 and 3.5). One of the outputs is connected to the input of the pulse generator, the other output can be used for the X-axis of the plotter.

An Intersil i8038 is used as the basis of the function generator. Since this unit may also be used in other applications, both sine and square function options of the i8038 are being used as well as the ramp function.

Figure 3.4 shows a stable $\pm$ 15 volt power supply for the function generator. Q103 is a by-pass transistor for the + 15 volts and Q101 is the voltage regulator for it. Q104 and Q102 are the corresponding transistors for the - 15 volts. + 15 V and - 15 V are connected to terminals L and X respectively as the supply voltages for the function generator (Figure 3.5).

On Figure 3.5 R111 is a current limiting resistor for the function generator chip. R113 is for the adjustable duty ratio. The capacitor bank, C104 through C111, gives a frequency choice of 10^5 Hz to 10^{-2} Hz. R112 is used as a fine frequency control. The distortion of the waveform can be minimized by the proper adjustments of R118 and R119. The output

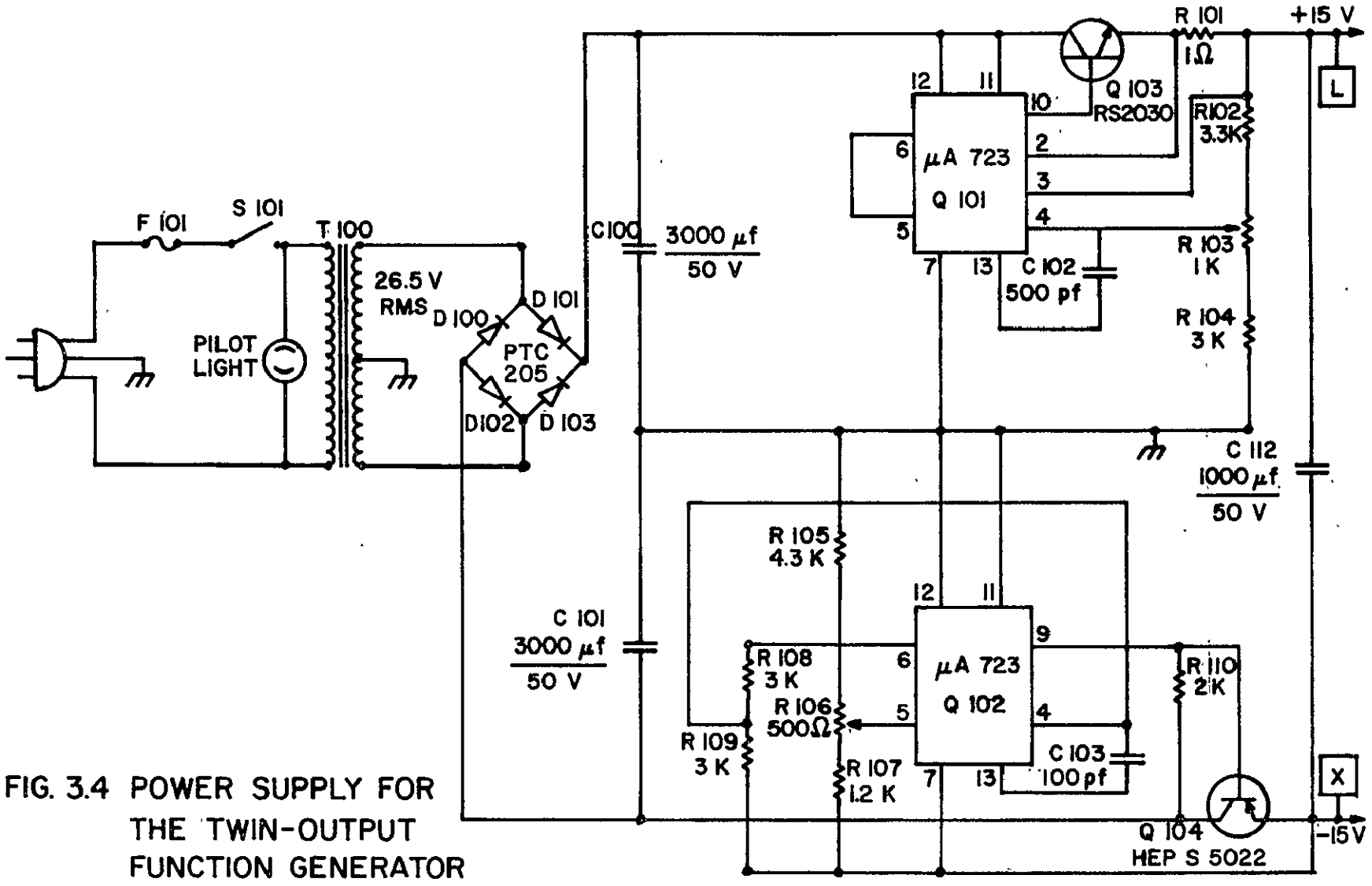

FIG. 3.4 POWER SUPPLY FOR THE TWIN-OUTPUT FUNCTION GENERATOR

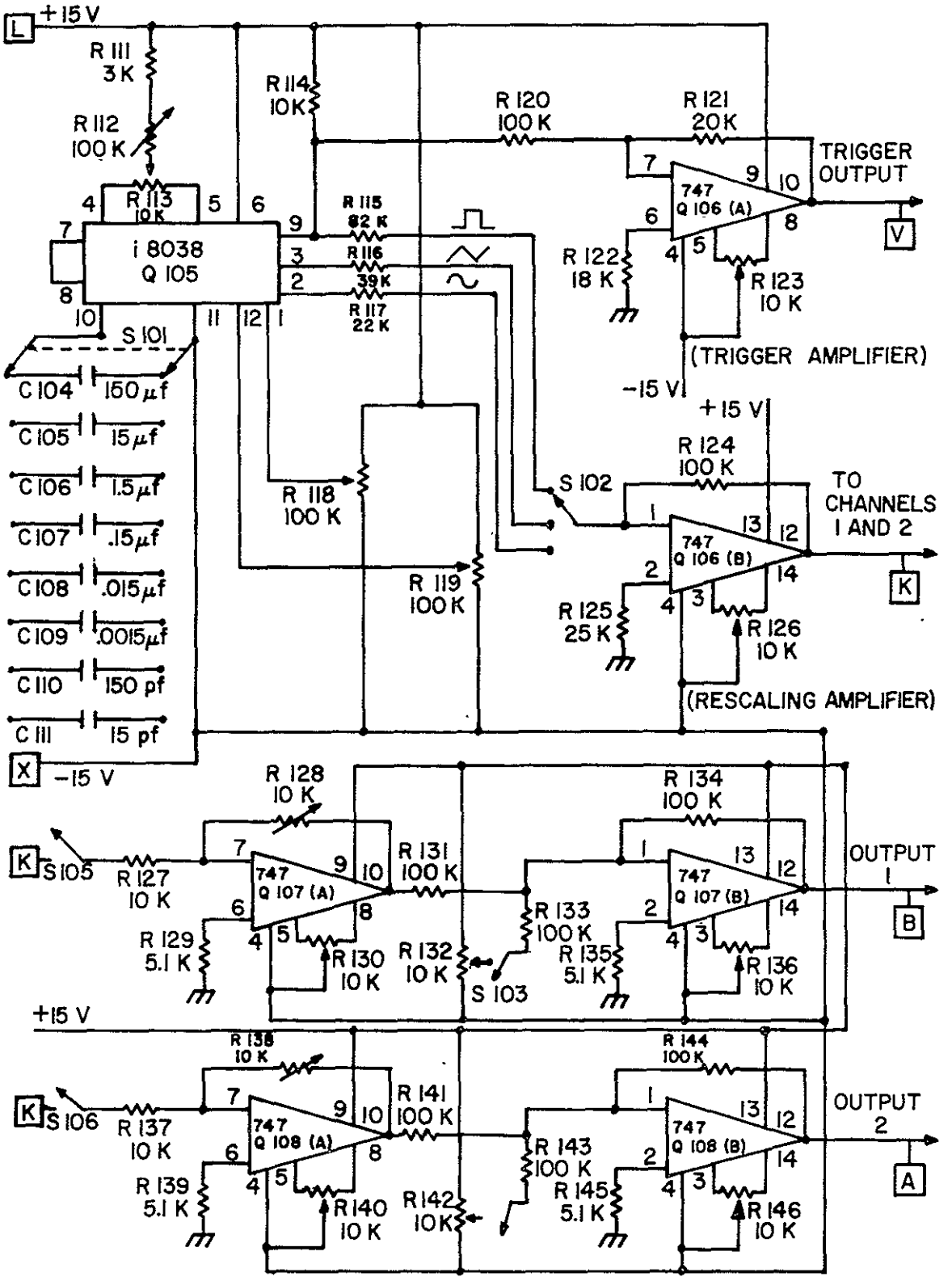

FIG. 3.5 SCHEMATIC DIAGRAM OF TWIN-OUTPUT FUNCTION GENERATOR

waveforms of the i8038 are of different magnitude. Therefore, resistors R115, R116, and R117 are used to rescale with Q106(B).

A triggered output is formed by taking the square wave at the load resistor R114 and coupling it through Q106(A).

The output of Q106(B) is separated into two channels. Channel 1 goes through the adjustable amplitude operational amplifier Q107(A) and the DC-bias amplifier Q107(B) to form output 1. Channel 2 goes through the adjustable amplitude operational amplifier Q108(A) and the DC-bias amplifier Q108(B) to form output 2. Resistors R128 and R138 are used for adjusting the amplitude of the function. R132 and R142 are used to adjust the DC-bias of the outputs.

All operational amplifers are dual 747 operational amplifier (Linear and Interface Circuits Data Book for Design Engineers, 1973).

3.3.2 Electrometer

The ion current from the ion source is detected by a Faraday cage (W. R. Miller and N. Axelrod, 1966) and fed to an electrometer. For higher frequency response, an electrometer was built which is similar to the one described by R. F. Reiter (1976).

The schematic diagram of the electrometer is shown in Figure 3.6. Switches S_1 and S_2 give a range of sensitivity from 10^{-9} Amp to 10^{-12} Amp full scale. The maximum output of the Keithley 302 is $\pm$ 10 Volts. An 1.0 mAmp meter protected by two 1n914 diodes is used for monitoring the output voltage of the Keithley 302.

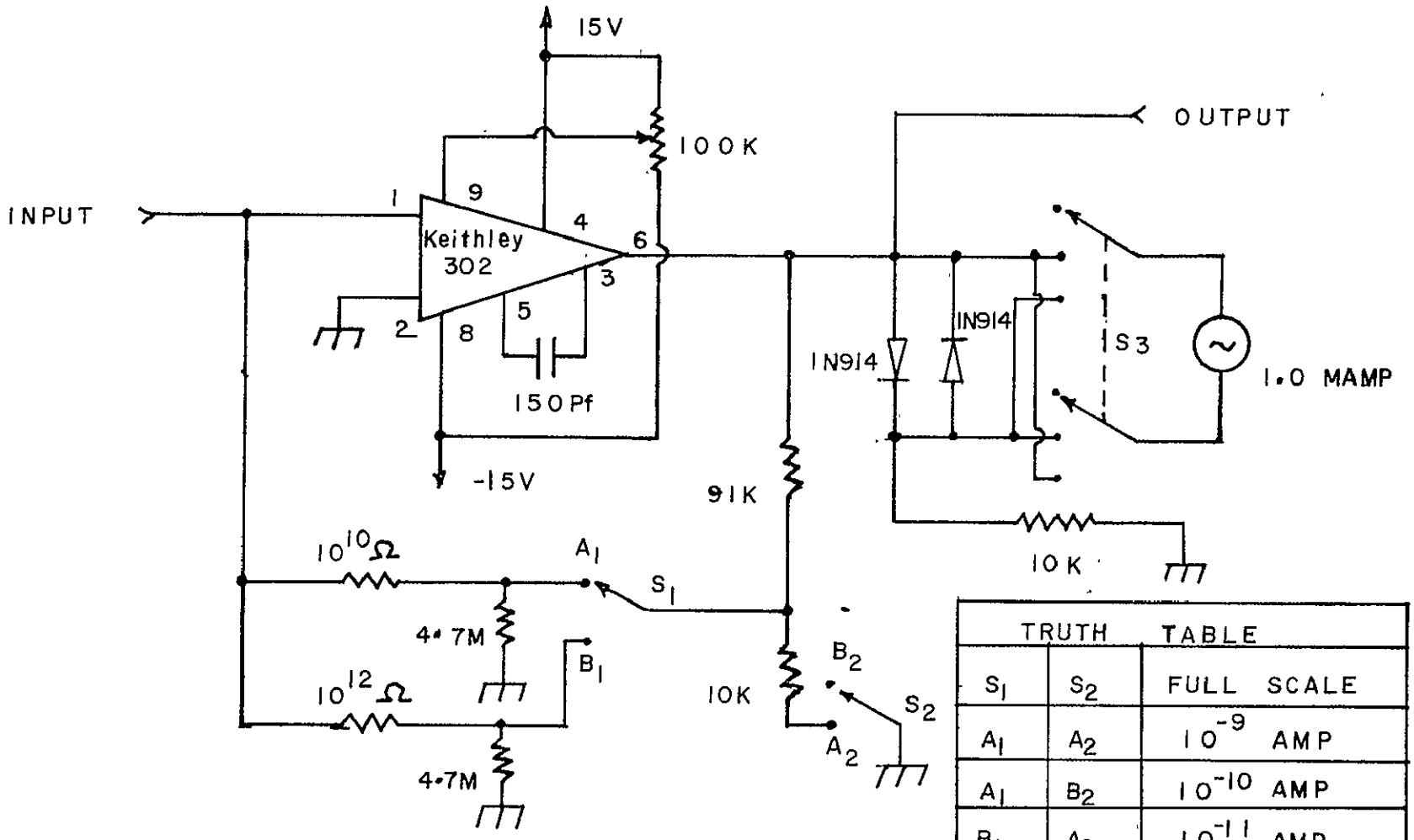

TRUTH TABLE		
S_1	S_2	FULL SCALE
A_1	A_2	10^{-9} AMP
A_1	B_2	10^{-10} AMP
B_1	A_2	10^{-11} AMP
B_1	B_2	10^{-12} AMP

Fig.3.6: Electrometer Circuit Diagram

CHAPTER IV

ACCELERATING MODE CONSTANT-MOMENTUM MASS SPECTROMETRY AS APPLIED TO A RESIDUAL GAS ANALYZER

4.1 Accelerating Mode I

The accelerating mode without gating was experimentally tested first. A schematic block diagram of the set up is shown in Figure 4.1. Ions are injected into the pulsing region from the ion source (see Section 3.2). Two pulses are used in this scheme; one on the first end plate and the other on the last end plate of the pulsing region. Both pulses have their magnitudes and widths fixed as shown in Figure 4.1. A set of five plates was used in the pulsing region to insure field uniformity. A set of resistors made of graphite lines on ceramic spacers were connected between the plates to drain away accumulated charges. A parallel plate analyzer is used and a triangular shaped wave is applied to it from Channel 1 of the function generator as the analyzing voltage.

Ions are then collected by a Faraday Cup whose outer shield is maintained at -90 volts to ground. This eliminates the slight effects of secondary electrons emitted when the primary ions strike the collector surface which is maintained at -60 volts to ground.

The collected signal is then fed to the electrometer (Figure 3.6). A filter (Figure 4.2b) is used for the signal output from the electrometer to eliminate high frequency oscillations and noises. A differentiator (Figure 4.2c) is used before the signal goes to the Y-axis input of the X-Y recorder. The X-axis input of the X-Y recorder is then swept by a triangular wave from Channel 2 of the function generator. The output

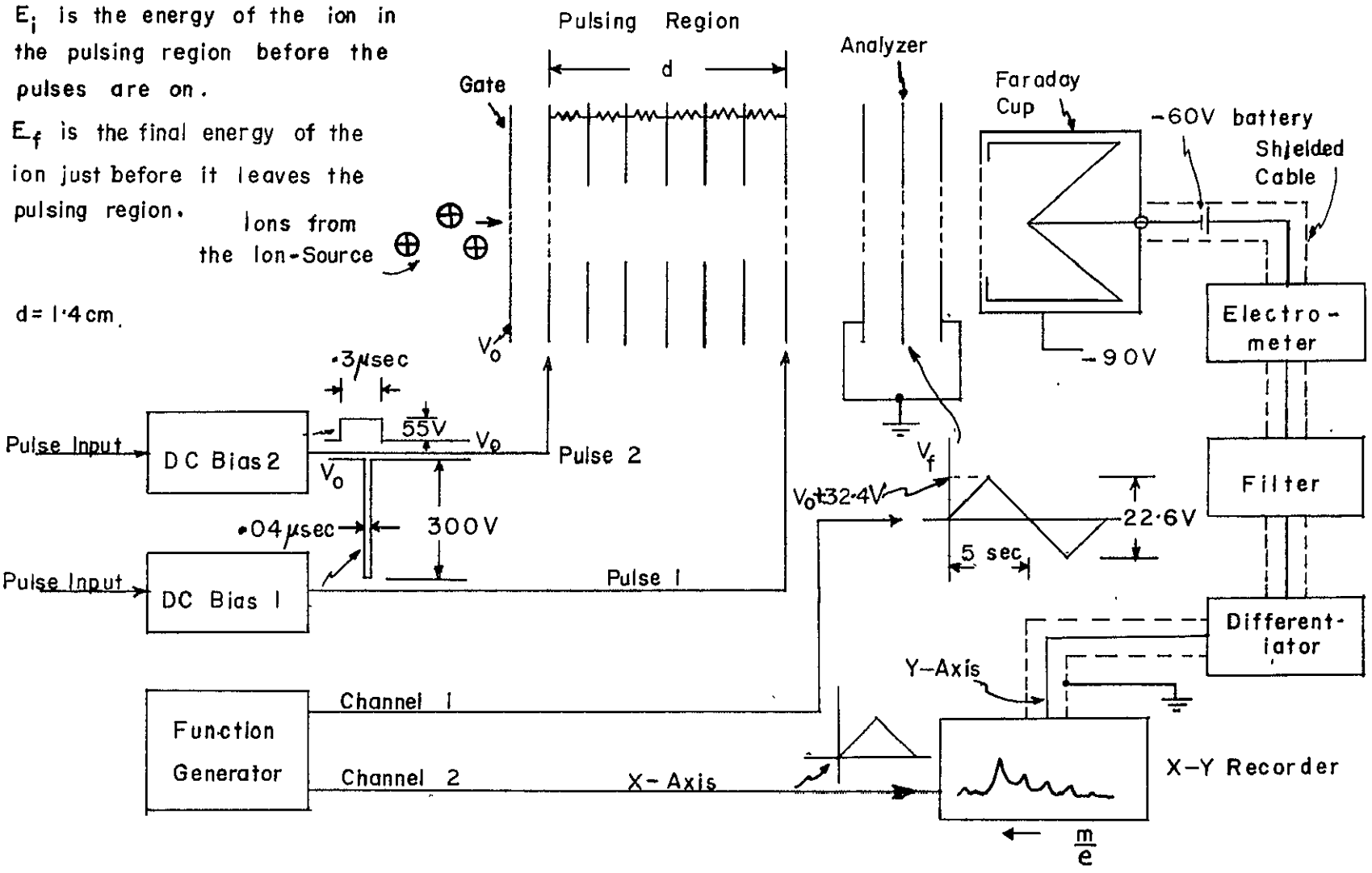

Fig.4.1: Block Diagram of Accelerating Mode I

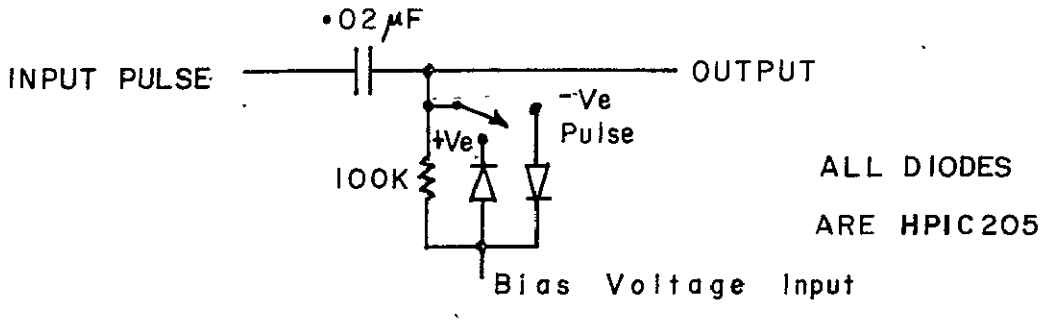

Fig.4.2.a: Schematic Diagram of the D.C. Bias

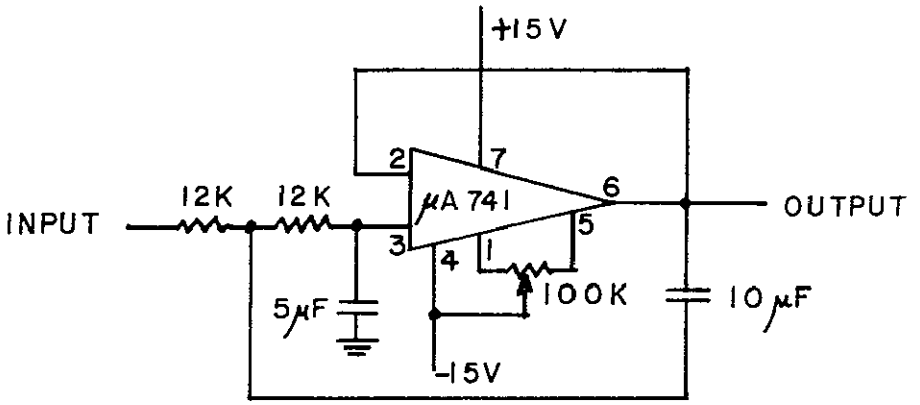

Fig.4.2.b: Schematic Diagram of the Filter

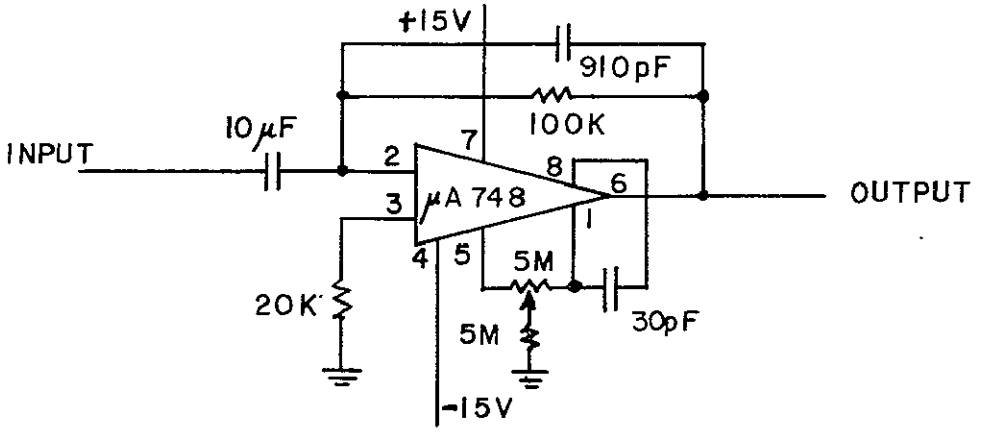

Fig.4.2.c: Schematic Diagram of the Differentiator

of the X-Y recorder then gives the derivative of ion current versus analyzer voltage. Since heavier masses gain less energy in this scheme, they show up to the left of the ligher masses in the mass spectrum.

A simple DC bias circuit (Figure 4.2a) is used to supply bias to the input pulses. In that circuit HPIC205 diodes are used (1000 volts peak voltage and a maximum current of 1 Amp).

As shown in Figure 4.3, before the pulses are turned on we obtain an initial ion energy, E_i, in the pulsing region of 1.5 eV and an initial ion energy spread, ΔE_i, equal to 0.7 eV. Before the pulses are turned on an ion current of approximately 10^{-9} Amp is obtained at a total pressure 5×10^{-5} Torr when an electron current of 10^{-4} Amp is applied. The mass spectra of argon and nitrogen are shown in Fig. 4.4. One gets a resolving power of about 5 for both nitrogen and argon which is approximately the same as predicted by theory. The sensitivity can be shown to be approximately 5×10^{-6} Amp/Torr with $I_{el} = 10^{-4}$ Amp, since only a narrow energy range of ions is used.

4.2 Accelerating Mode II

When a gating pulse is applied to the gate before the pulsing region (Figure 4.5), better control of the ions is achieved. In the scheme illustrated in Figure 4.5, one gets $E_i = 2.56$ eV and $\Delta E_i = 1.06$ eV. The heavier masses gain less energy and show up to the left of the lighter masses in the mass spectrum.

The mass spectra of argon and nitrogen are shown in Figure 4.6. The experimental resolving power at mass 28 is approximately 7.7 and that at mass 40 is about 6.9. These results are also comparable to

Horizontal Axis: E_i, 1 inch = 2·26eV.

E_i is the initial energy of the ions in the pulsing region.

Vertical Axis: $\frac{dI_{ion}}{d\tau}$ in arbitrary scale, τ is the time.

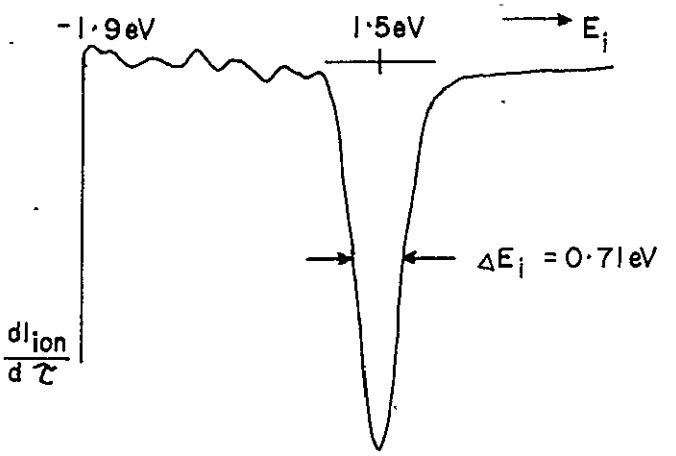

Fig. 4.3: Test on Initial Energy of Ions with a Triangular Wave at the Analyzer

E_i = 1·5eV, ΔE_i = 0·71eV,

E_{cA} = 7·9eV, E_{cN_2} = 11·4eV

Horizontal Axis: E_f, 1 inch = 3·01 Volts.

E_f is the final energy of the ion just before it leaves the pulsing region.

Vertical Axis: $\frac{dI_{ion}}{d\tau}$ in arbitrary scale. τ is time.

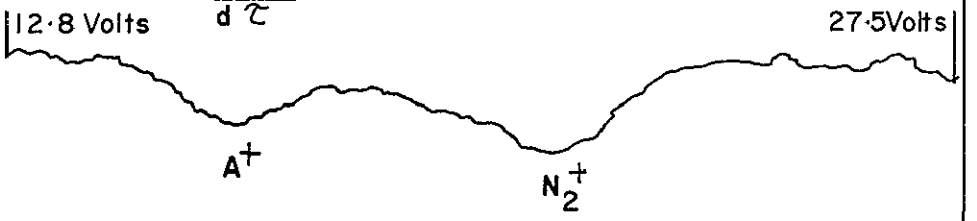

Fig. 4.4: Mass Spectrum of Argon and Nitrogen obtained with Accelerating Field CMMA Mode I

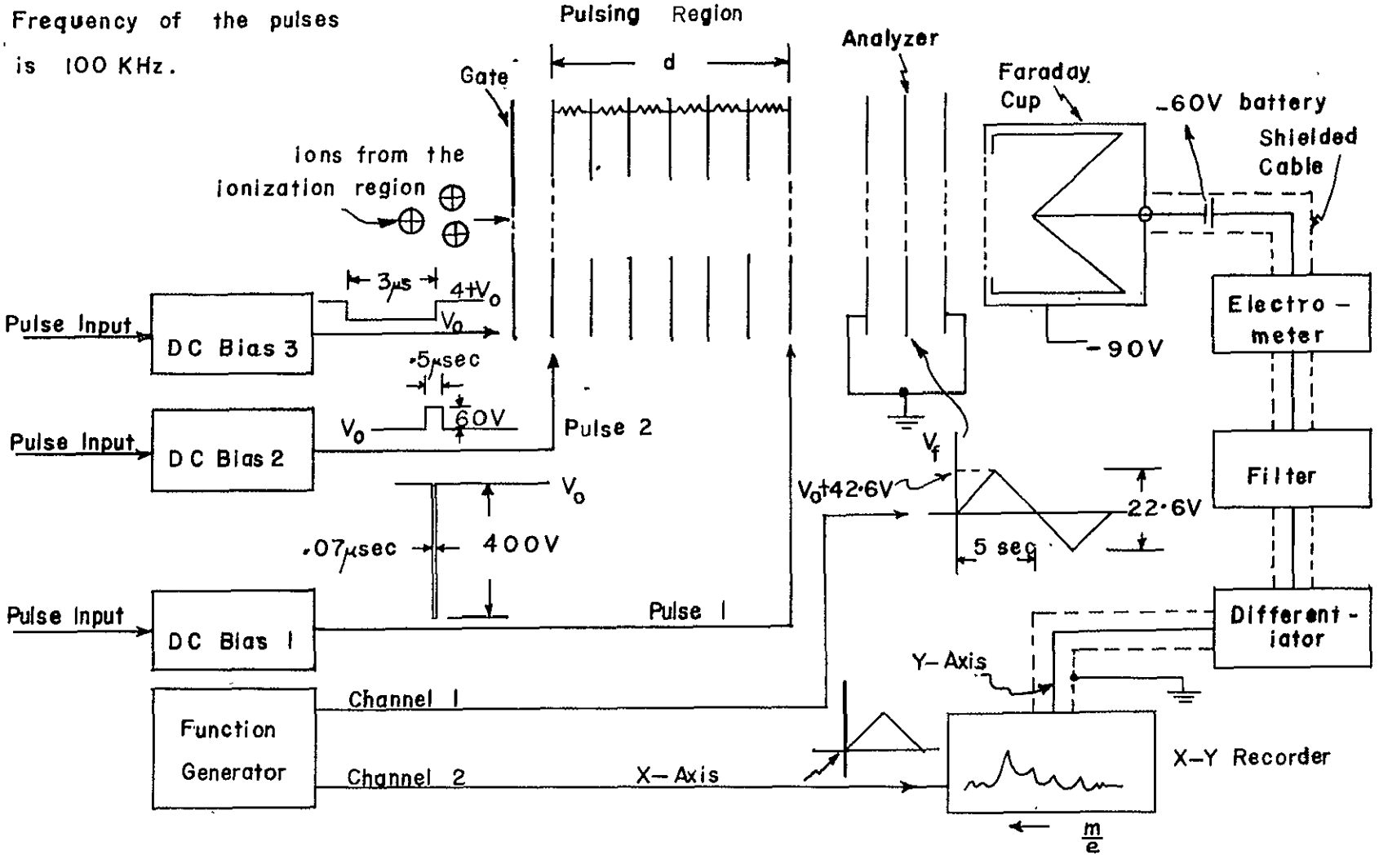

Fig. 4.5: Block Diagram of Accelerating Mode II

E_i = 2·56 eV, ΔE_i = 1·06 eV.

Horizontal Axis : E_f, 1 inch = 3·01 Volt.

E_f is the energy of the ion just before it leaves the pulsing region.

Vertical Axis : $\frac{dI_{ion}}{dt}$ in arbitrary scale. t is time.

$E_{cA} \cong 15{\cdot}2$eV, $E_{cN_2} \cong 21{\cdot}7$eV.

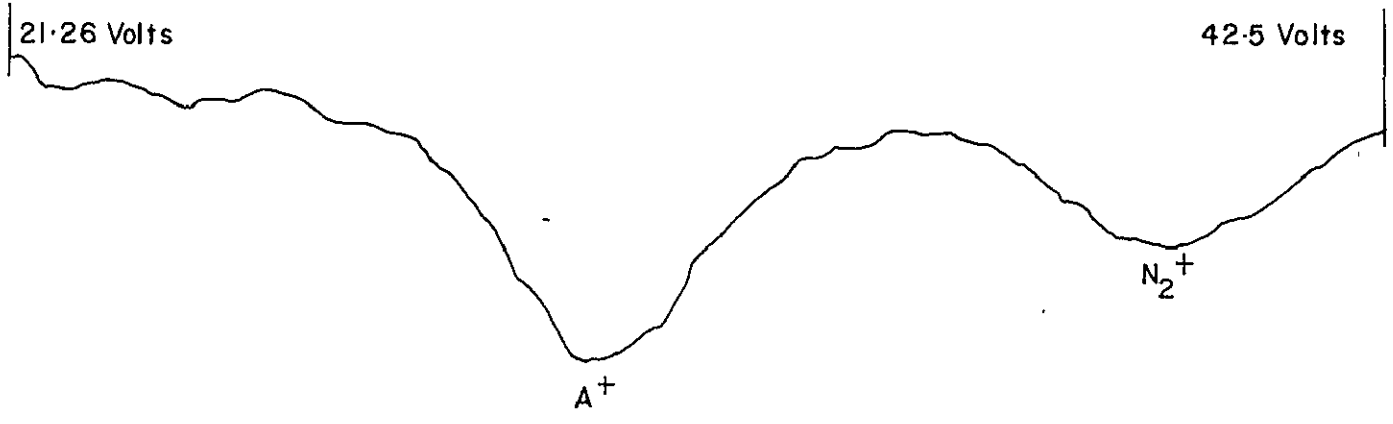

Fig.4.6 : Mass Spectrum of Argon and Nitrogen obtained with Accelerating Field CMMA Mode II

those predicted by theory. However, the final energy spread ΔE_f of the ions becomes larger, making it more difficult to get a spectrum of wider mass range. Moreover, in this scheme the resolving power is mass dependent, the lighter masses being better resolved.

The ion current being detected is on the order of 10^{-9} Amp when an electron current of 10^{-4} Amp is applied at a pressure of 5×10^{-5} Torr. The sensitivity of this scheme is better than that of the accelerating mode I and is of the order of 10^{-5} Amp/Torr for argon, since a wider energy range of ions is used.

4.3 Accelerating Mode III

In order to minimize the mass dependence of the resolution, the scheme indicated in Section 2.4 is used. The block diagram of this basic operation is shown in Figure 4.7. Also, in order to give a better resolution, E_i is increased to a higher value, as discussed at the end of Chapter 2.

A Velonex Model V-1589 Pulse Generator was used in this scheme. It is capable of producing a pulse of varying width t, when a varying voltage is applied to its variable-width input. This can be achieved by using Channel 1 of the function generator while Channel 2 is sweeping the X-axis of the X-Y recorder. The pulse of varying width (Pulse 1) is then applied to the first end plate of the pulsing region (Figure 4.7) while the analyzer's voltage V_f is kept at a constant value. Lighter ions will gain enough energy to pass through the analyzer first, and will show up to the left of the heavier ones in the mass spectrum.

The mass spectrum of a mixture containing predominantly argon and nitrogen is shown in Figure 4.8. E_i in this case is about 47.3 eV and

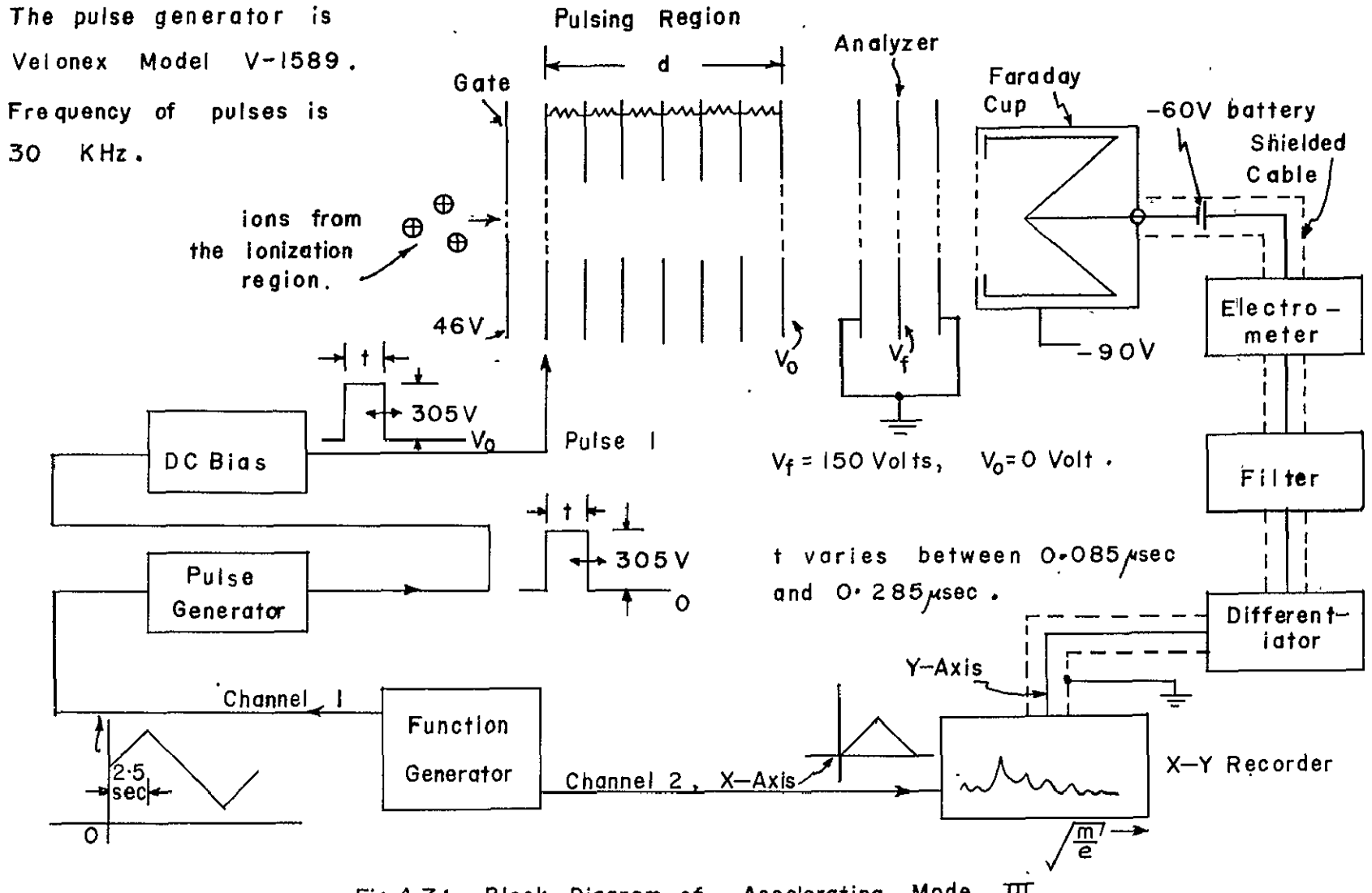

Fig. 4.7: Block Diagram of Accelerating Mode III

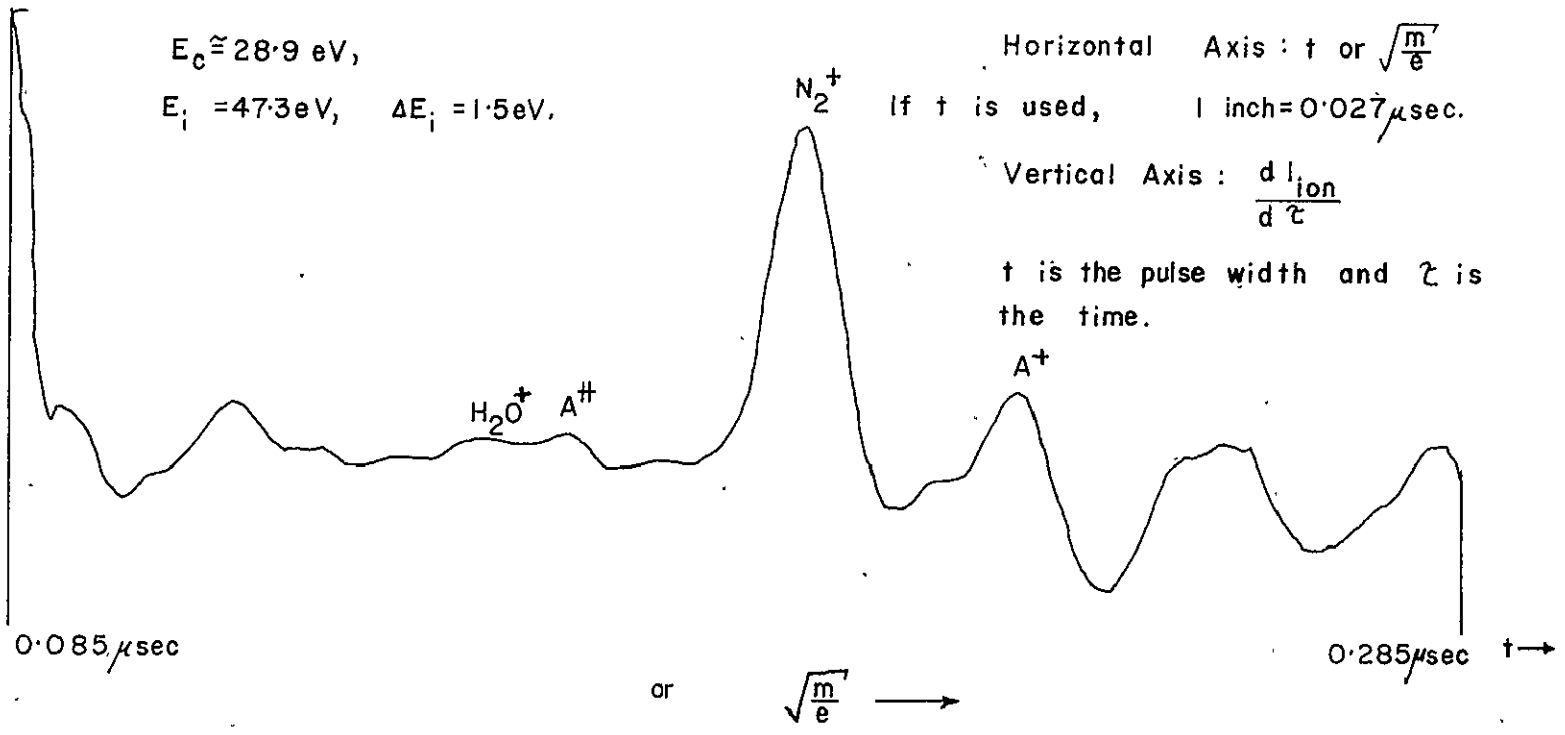

Fig.4.8: Mass Spectrum of mainly Nitrogen and Argon obtained with Accelerating Field CMMA Mode III

ΔE_i is about 1.5 eV. The resolving power of both nitrogen and argon is equal to 10.5. However, since V_f is maintained at 150 volts relative to the DC pulsing region potential V_o (in this case, V_o equals ground potential), the energy resolution, ε, of the analyzer becomes a major factor affecting the mass resolution.

When the pulse width, t, varies from 0.085 μ seconds to 0.285 μ seconds, the mass spectrum covers a range of m/e from 6 to about 65 (m is the number in amu and e is the number of positive charges that the ion carries). Sensitivity of this mode of operation is only about 10^{-6} Amp/Torr with an electron current of 10^{-4} Amp, since the frequency of the pulses can only extend to 30 KHz (duty ratio of the Velonex pulse generator is only 1%). A waveform eductor, added after the differentiator, only improves the situation slightly.

4.4 Accelerating Mode IV

In order to obtain better control of the ion current, a gating pulse is added to the scheme of accelerating mode III. The block diagram of this scheme is shown in Figure 4.9. Here, lighter masses will again gain enough energy to pass the analyzer before the heavier masses. As before, lighter masses will show up to the left of the heavier masses in the mass spectrum.

The mass spectrum of a mixture containing predominantly argon and nitrogen is shown in Figure 4.10. In this case E_i = 47.3 eV, ΔE_i = 1.5 eV, while E_f is maintained at 130 volts relative to the DC potential V_o of the pulsing region. One obtains a resolving power of about 10 for this mixture. The effect of the energy resolution of the analyzer, ε, is found to be less significant here than in accelerating mode III

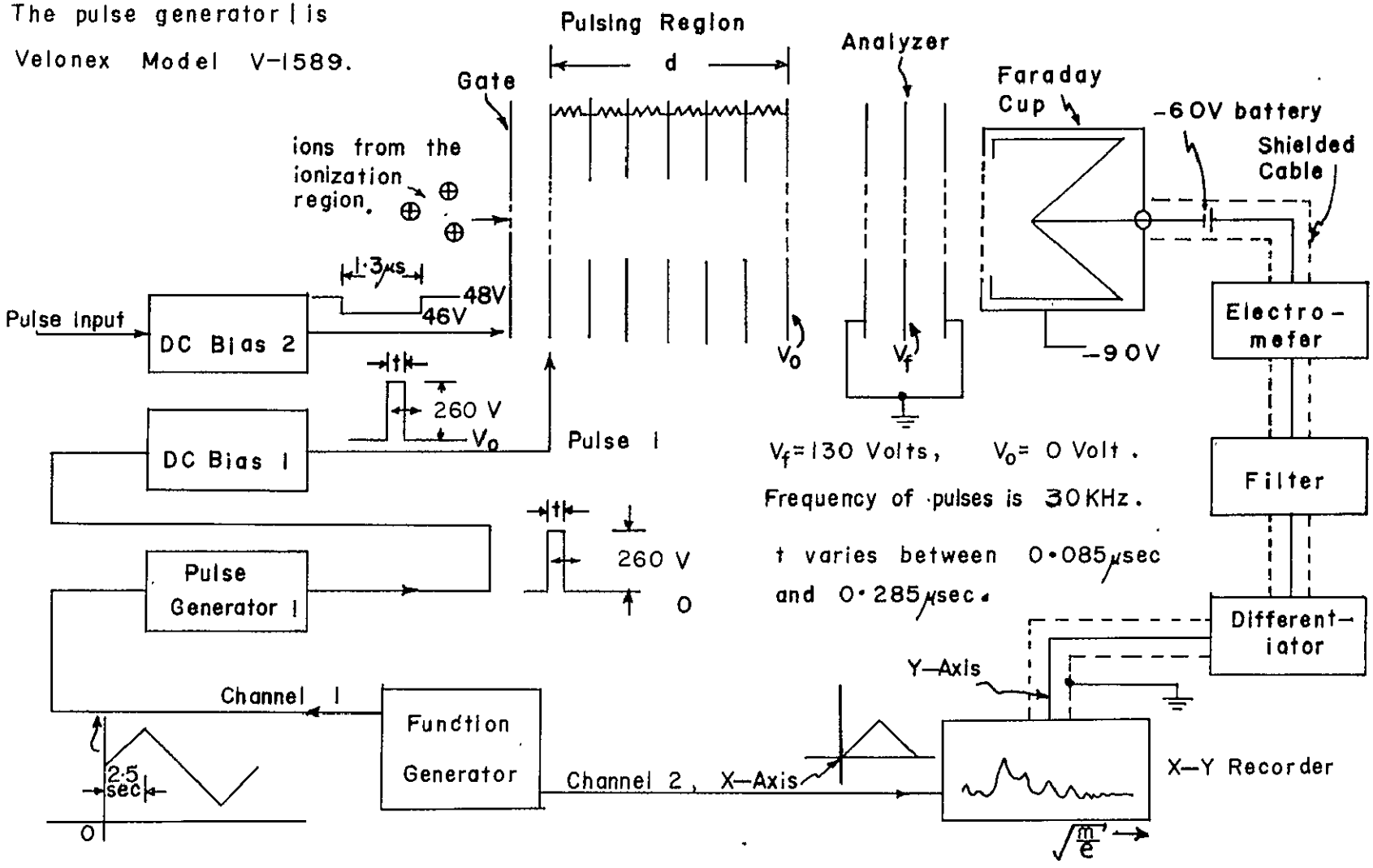

Fig.4.9: Block Diagram of Accelerating Mode IV

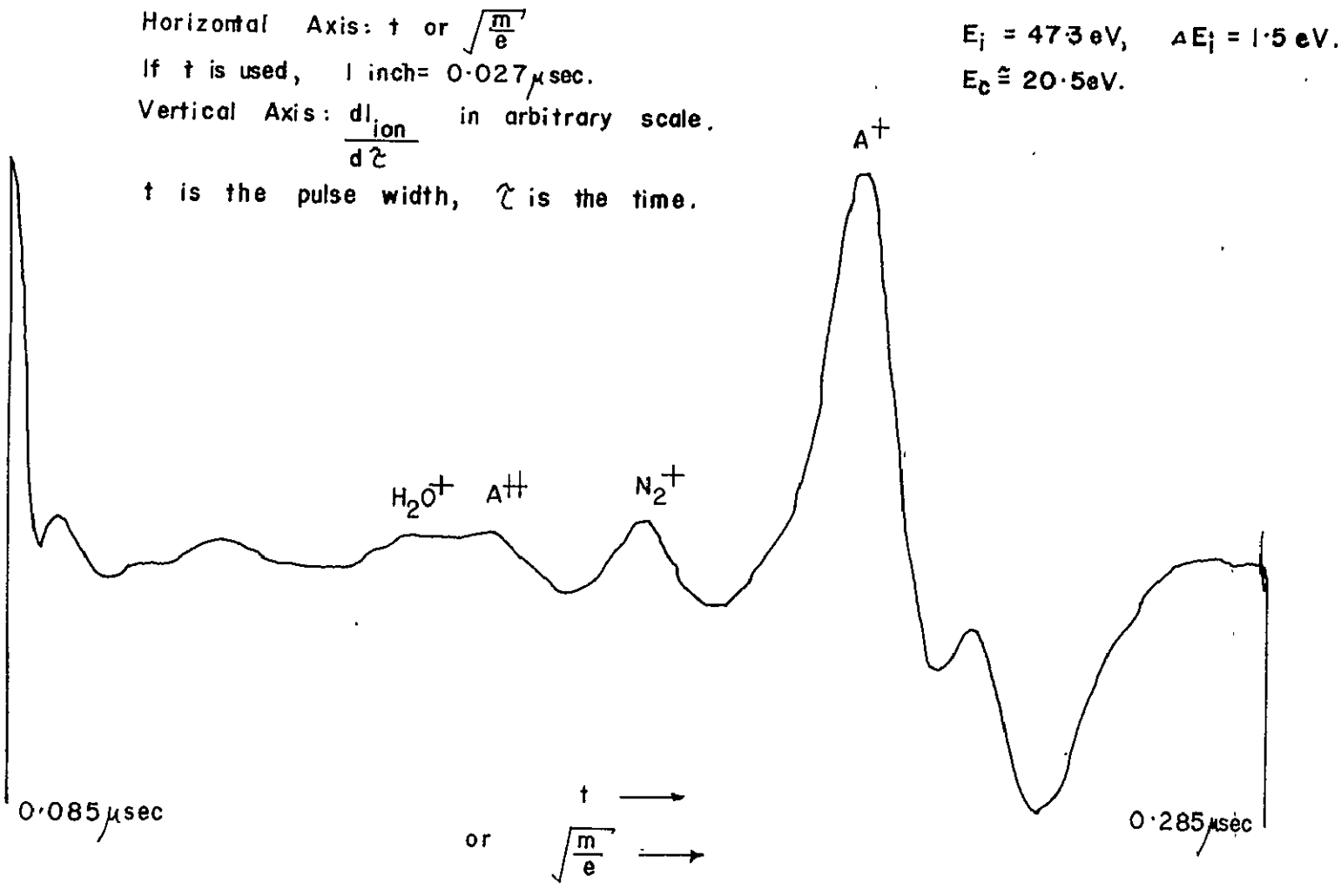

Fig. 4.10: Mass Spectrum of mainly Argon obtained with Accelerating Field CMMA Model IV

(possibly due to decrease in E_f). When the pulse width, t, varies between 0.085 μ seconds to 0.285 μ seconds, it covers a range of m/e from 6 to about 67. It is possible that the resolution may also be limited by the response of the filter, differentiator and the X-Y recorder. Sensitivity in this scheme is about 10^{-6} Amp/Torr with an electron current of 10^{-4} Amp. Again, usage of a waveform eductor helps only slightly.

CHAPTER V

DECELERATING MODE CONSTANT-MOMENTUM MASS SPECTROMETRY AS APPLIED TO A RESIDUAL GAS ANALYZER

5.1 Decelerating Mode I

Here, as shown in Figure 5.1, one uses a scheme similar to the one used in accelerating mode II. A gating pulse is used, and then a decelerating pulse of fixed width is applied to the last end plate of the pulsing region. A triangular waveform is applied to the analyzer from Channel 1 of the function generator. Since lighter masses lose more energy, they will have a lower energy and will show up to the left of heavier masses in the mass spectrum.

A filter and a differentiator are used in this method. The Y-axis of the X-Y recorder will show the derivative of the ion current. The X-axis will show the analyzer voltage V_f when a triangular wave from Channel 2 of the function generator is applied to it.

A mass spectrum of an argon-nitrogen mixture is shown in Figure 5.2. The resolving power at m/e equals to 40 is about 3 which is close to what theory predicts. E_i in this case is 21.6 eV and ΔE_i = 1.5 eV.

One also notices that the final energy spread, ΔE_f, of the ions does not deteriorate as in the case of all accelerating modes. Although a decrease in the half width of the mass peaks is not actually observed, it can be accounted for by the leakage of ions to the detector during the beginning and end of the gating pulse. The sensitivity in this scheme is about 2×10^{-6} Amp/Torr which is not too bad relative to the accelerating modes. In order to get a higher resolution, one has to increase E_i, and in order to avoid the resolution's mass dependence, one can keep V_f a constant but vary the width t of the pulse (See Section 2.6).

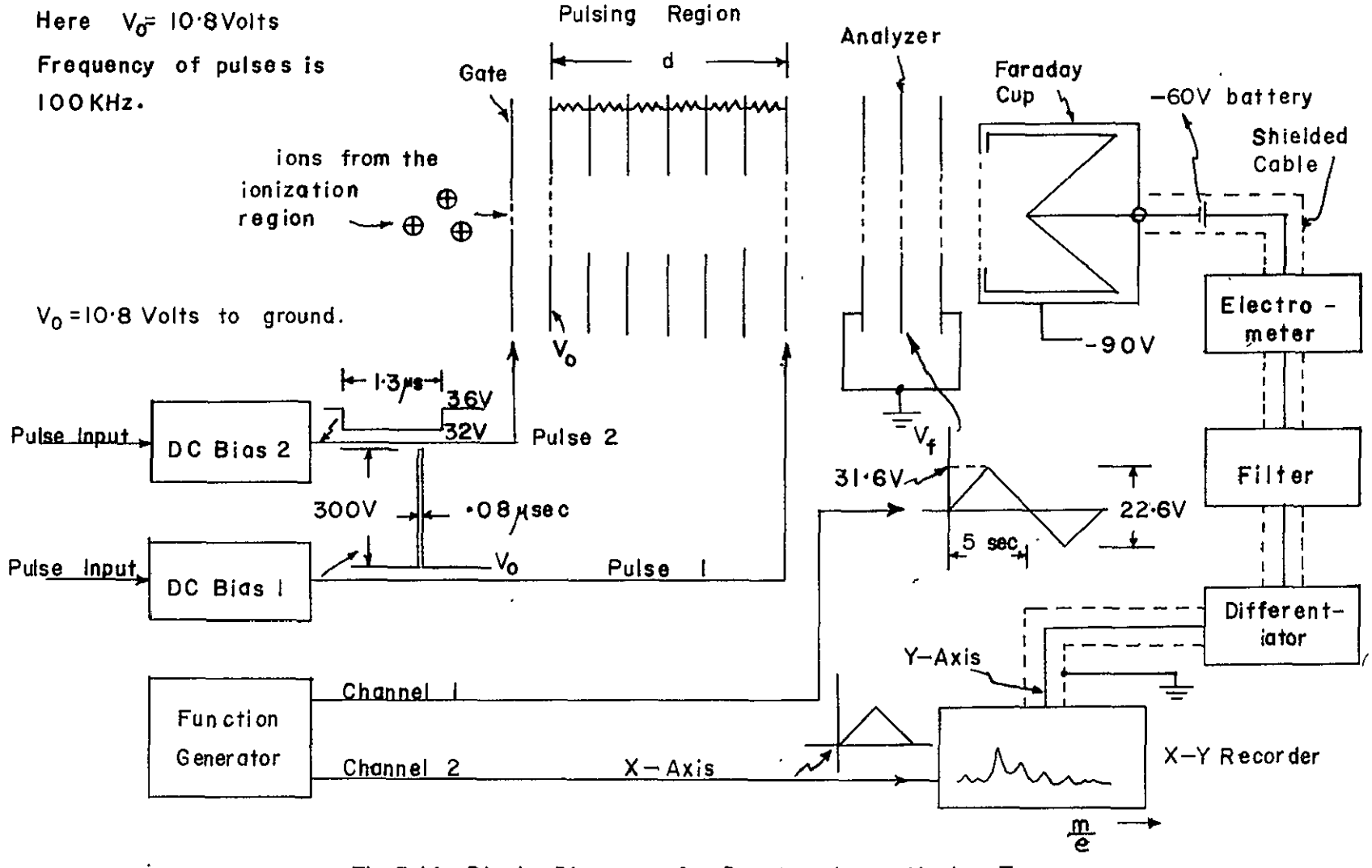

Fig.5.1: Block Diagram of Decelerating Mode I

$E_i = 21{\cdot}6\ eV, \quad \Delta E_i = 1{\cdot}5\ eV$.

$E_{cA} = 2{\cdot}9 eV, \quad E_{cN_2} = 4{\cdot}14\ eV$.

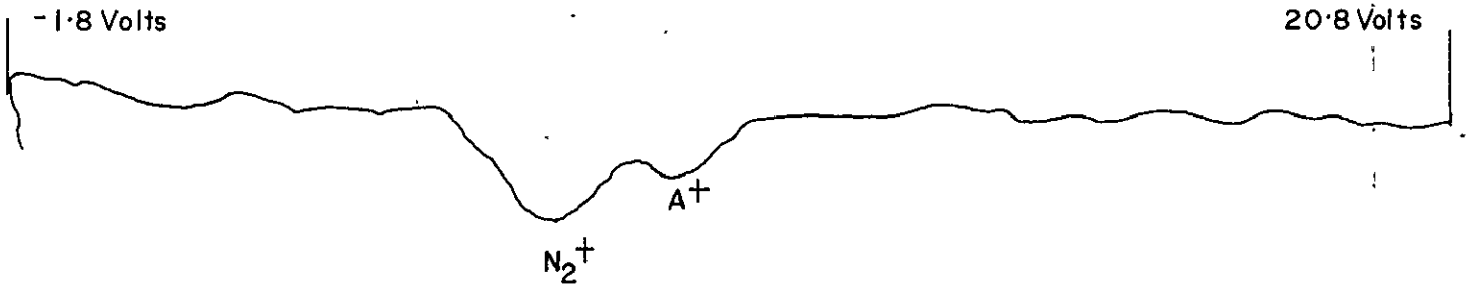

Horizontal Axis: E_f , 1 inch = 3·04 Volts .

E_f is the final energy of the ion just before it leaves the pulsing region .

Vertical Axis : $\frac{dI_{ion}}{d\tau}$ in arbitrary scale, τ is time.

Fig.5.2 : Mass Spectrum of Argon and Nitrogen obtained with Decelerating Field CMMA Mode I

5.2 Decelerating Mode II

In this scheme, E_i has been increased to 50.8 eV and ΔE_i is measured as 1.8 eV. The method is illustrated in Figure 5.3. A gate pulse is used and there is a time delay between the gate pulse and the decelerating pulse (Pulse 1). Essentially only the ions between the gate and the first end plate of the pulsing region are used. The initial ion energy is measured only with the gate pulse on. Therefore, one can choose the width of the gate pulse to achieve optimum conditions. A time delay between the gate pulse and the decelerating pulse is necessary in order to let the ions into the pulsing region before they are decelerated.

The variable width pulse is supplied by the Velonex V-1589 pulse generator. The pulse width, t, is varied according to a triangular wave input to the pulse generator from Channel 1 of the function generator. V_f in this case is maintained at 5.6 volts relative to the DC pulsing region potential V_o. As has been pointed out in Section 2.6, this ensures the maximum resolving power possible for E_i = 50.6 eV, and ΔE_i at 1.8 eV. However, this is only an estimation experimentally, since one doesn't exactly know the value of the energy resolution, ε, of the analyzer.

Ions of lighter masses lose more energy and will be stopped by the analyzer earlier than the heavier masses, therefore, lighter masses will show up to the left of the heavier ones in the mass spectrum. The Y-axis of the X-Y recorder shows the derivative of ion current with respect to time, and the X-axis is swept by a triangular wave from Channel 2 of the function generator.

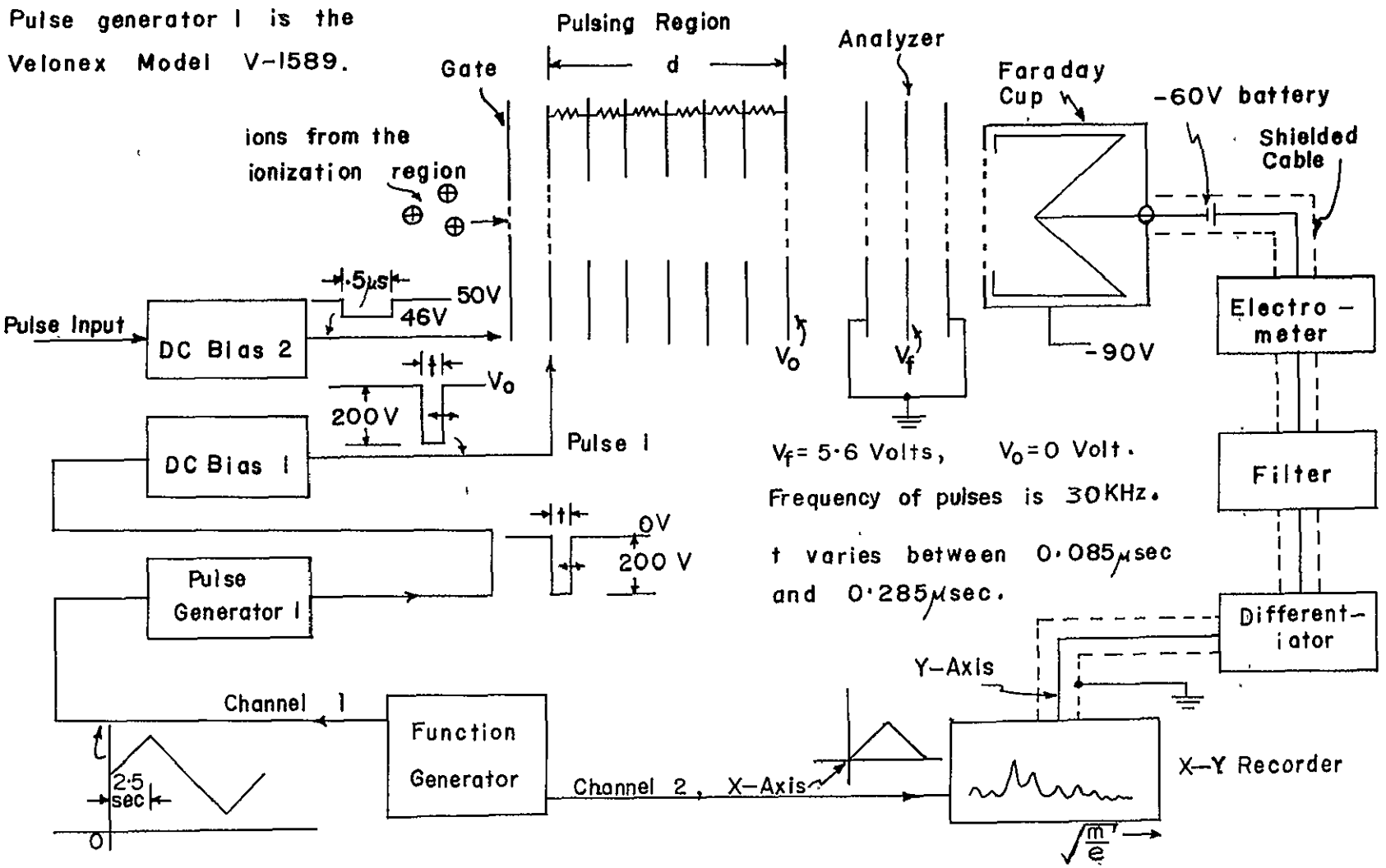

Fig. 5.3 : Block Diagram of Decelerating Mode II

Horizontal Axis : t or $\sqrt{\frac{m}{e}}$

If pulse width t is used, 1 inch = 0·027 sec.

Vertical Axis : $\frac{dI_{ion}}{d\tau}$ in orbitrary scale.

τ is the time.

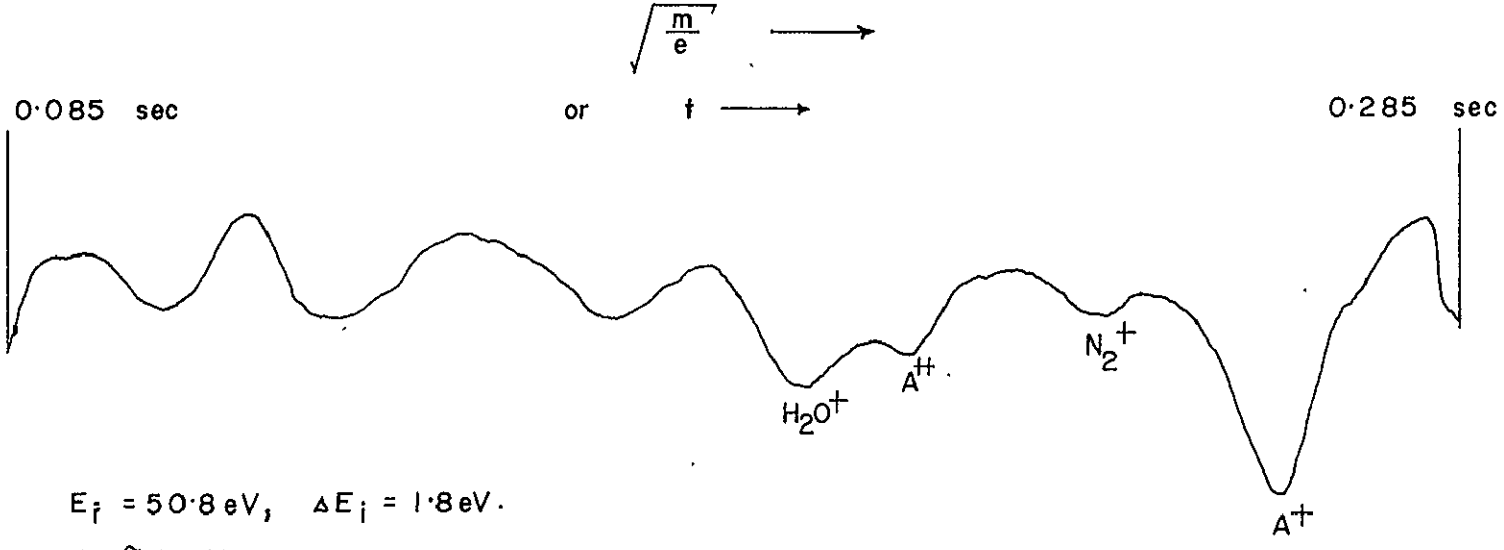

E_f = 50·8 eV, ΔE_i = 1·8eV.

$E_c \cong$ 18eV.

Fig.5.4: Mass Spectrum of mainly Argon obtained with decelerating Field CMMA Mode II

A mass spectrum of predominantly argon-nitrogen mixture is shown in Figure 5.4. A resolving power of 8 to 10 is obtained which is comparable to what theory predicts. Once again, one notices that ε will play an important role. Ironically, however, ε will be small as V_f is small. When t varies from 0.085 μ seconds to 0.285 μ seconds, the mass spectrum covers a m/e range of 4 to about 44. The sensitivity in this scheme is about 2×10^{-7} Amp/Torr. This is mainly because one only uses a small portion of the ions between the gate and the first end plate of the pulsing region. One thing that must be noted is that the resolution in this decelerating mode is comparable to those of the accelerating modes III and IV, although the sensivitity is lower. However, in this case, the number of ions being pulsed is strongly mass dependent. The waveform eductor helps more in this case than the accelerating modes.

The resolution is also limited by the responses of the filter, differentiator, and the X-Y recorder. The flight path of ions in the above two decelerating modes as well as the accelerating modes (I, II, III, IV) is only 6.6 cm.

CHAPTER VI

CONCLUSIONS, COMMENTS, AND SUGGESTIONS

6.1 Conclusions

A resolving power of about 10 to 11 can be obtained in the accelerating and the decelerating modes of this residual gas analyzer. It was found that the resolving power increases as E_i increases, as E_c increases, and as ΔE_i decreases (as predicted in the conclusion of Chapter II). With a reasonable voltage of 200 volts and variable pulse width, t, from 0.085 μ seconds to 0.285 μ seconds; one can get as shown in Section 5.2 a reasonable resolving power of about 10. The system can operate up to a pressure of 5×10^{-3} Torr without deterioration. The sensitivity of the system varies from 10^{-5} Amp/Torr to 2×10^{-7} Amp/Torr depending on which mode is used.

It was also found that the resolution for the decelerating mode (Section 5.2) can be comparable to that of the accelerating modes. The energy resolution, ε, of the analyzer is also a very important factor.

This system could be used as a nonmagnetic residual gas analyzer in the ionosphere from 250 Km to 80 Km. Its main advantages are: reasonable resolution and sensitivity, an extremely short flight path for ions (6.6 cm), compactness and simplicity of operation.

A picture of the gas analyzer, electronics and the vacuum system is shown in Fgiure 6.1. Another picture of the ion source and the gas analyzer itself with a triangular bandpass filter is shown in Figure 6.2.

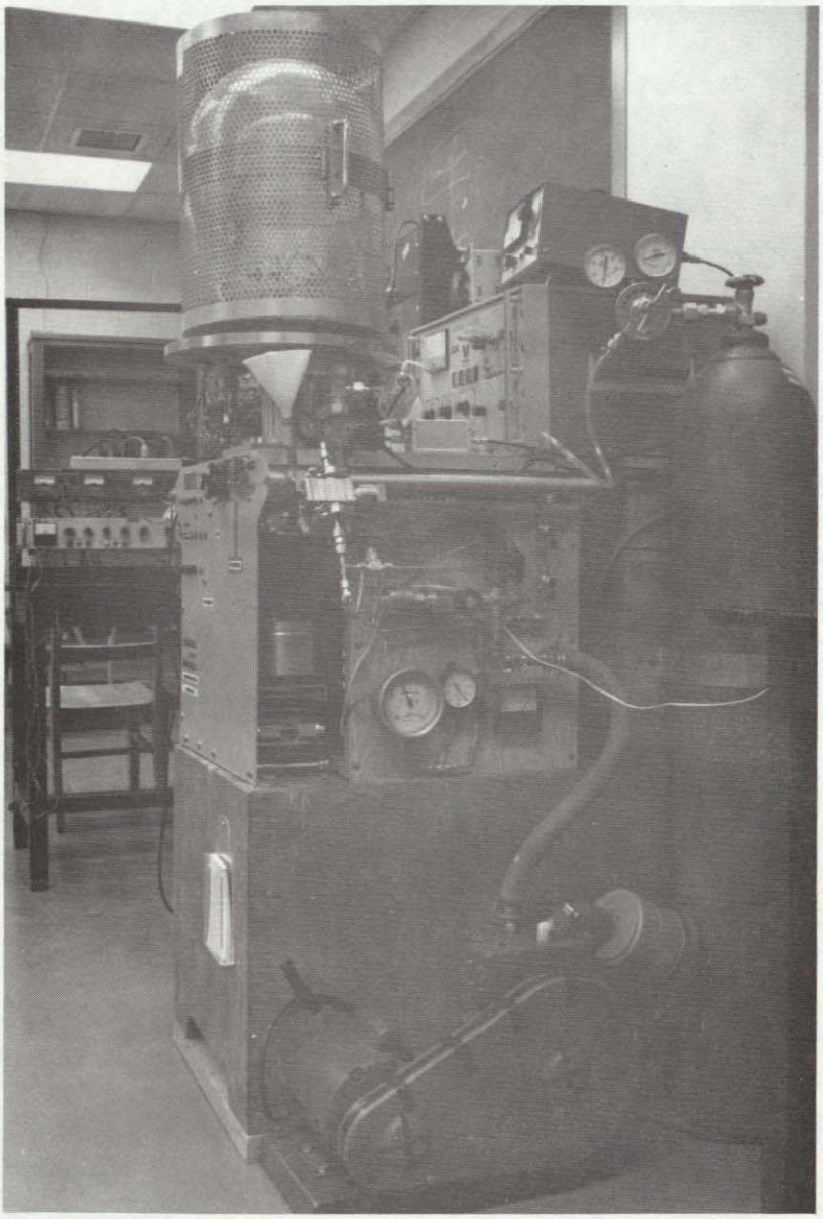

Fig.6.1 Photograph of the Experimental Setup (including the Vacuum System, relating Electronics and the Gas Analyzer itself.)

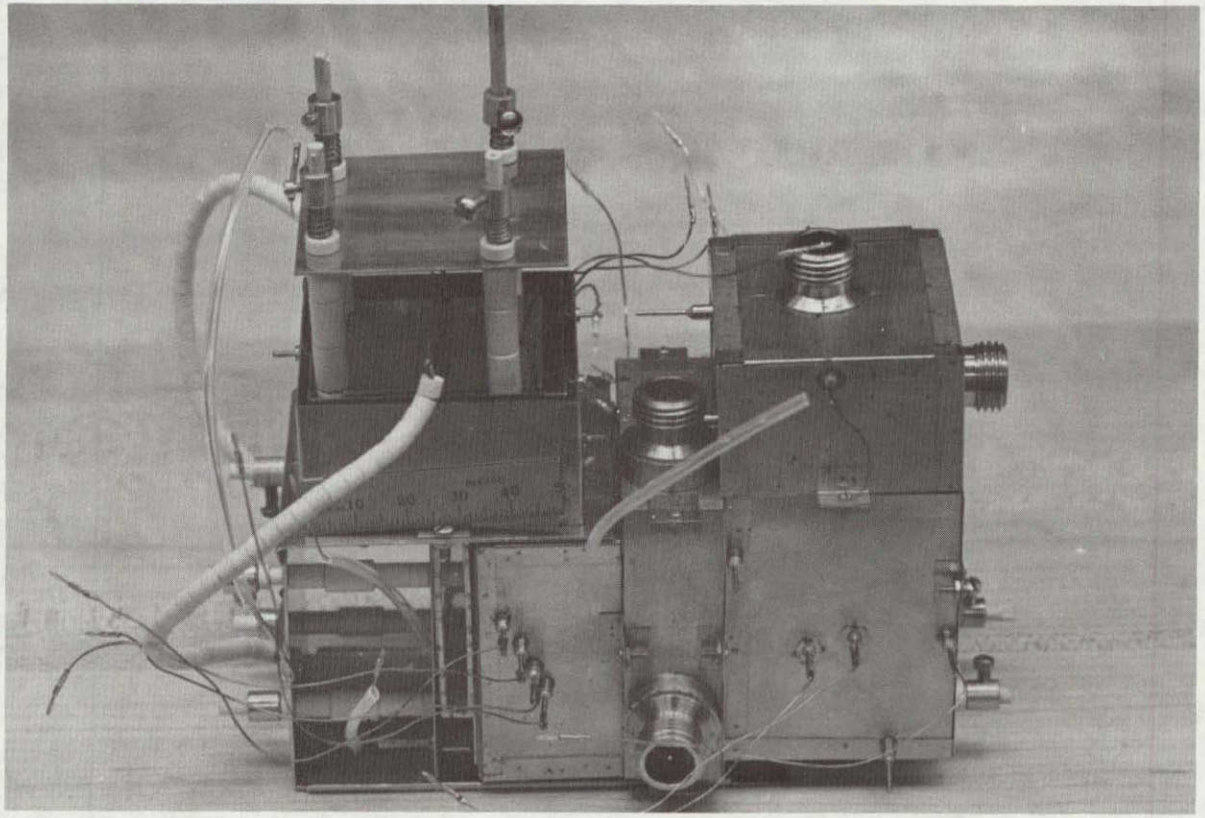

Fig. 6.2: Picture of the Residual Gas Analyzer with a Triangular Bandpass Filter as the Voltage Analyzer

6.2 Comments and Suggestions

As pointed out in Section 6.2, although the resolution of the decelerating mode constant-momentum mass spectrometer is comparable to that of the accelerating mode, the sensitivity of the decelerating mode is usually lower. One might even get a higher sensitivity for both cases if the modifications illustrated in Figures 6.3a, 6.3b, 6.4a, and 6.4b are used.

First of all, using a nonmagnetic sector field (which may be cylindrical or spherical), one can eliminate the differentiator which is not that useful when the sweep is slow. Secondly, as pointed out by Steckelmacher (1973), a screenless analyzer is usually better than an analyzer with screens, especially when the ion energy is small. Therefore I would suggest that it should be used in the modified versions of gas analyzer as shown in Figures 6.3a, 6.3b, 6.4a, and 6.4b.

Figures 6.3a and 6.3b refer to the accelerating mode. For Figure 6.3a, (first suggested by Dr. B. R. F. Kendall) there are two applied pulses. When pulse 2 is on, it stops the electron beam from reaching the ionization region. Subsequently, an accelerating pulse of varying width is applied as Pulse 1 while ions are analyzed by the sector field analyzer. Ions are contained in the ionization region before Pulse 2 is on by a DC bias voltage on the two plates which form the ionization region (as shown in Figure 6.3a).

In the system illustrated in Figure 6.3b, electrons are injected directly into the pulsing region and the electron beam axis is parallel to the ion beam axis. Although the cylindrical or spherical analyzer can eliminate some photo-ionization inside the analyzer region, one still expects a leakage ion current. However, the sensitivity of

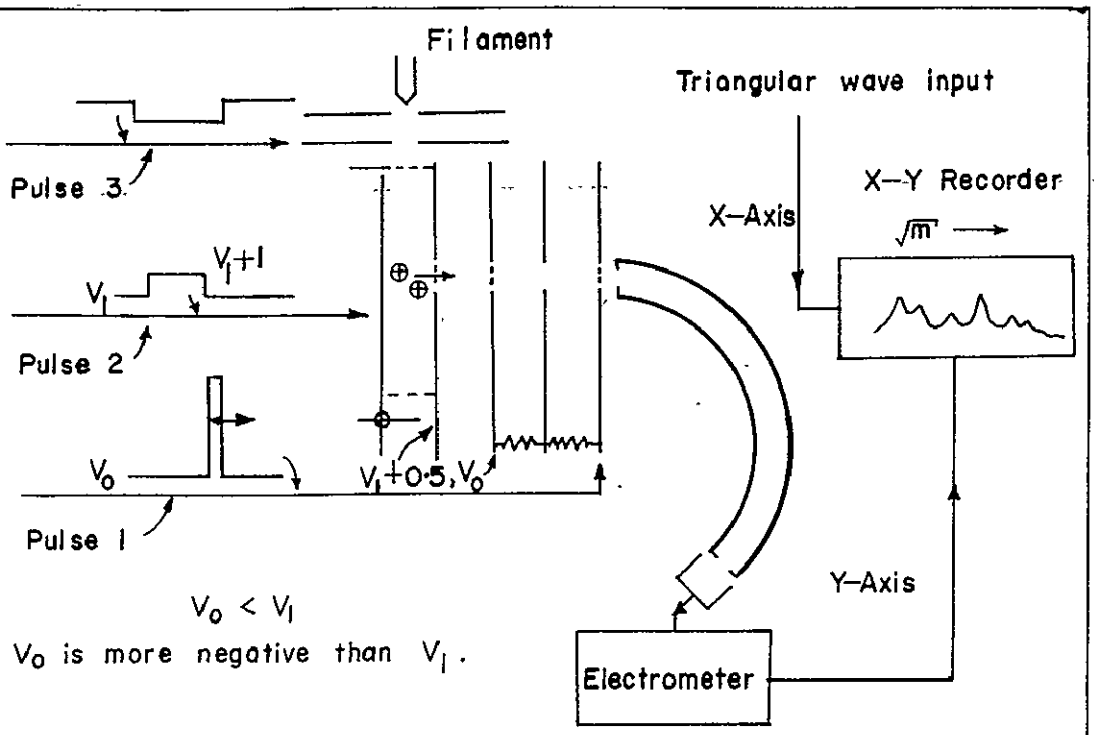

Fig.6.4.a: Block Diagram of Suggested Decelerating CMMA Mode I

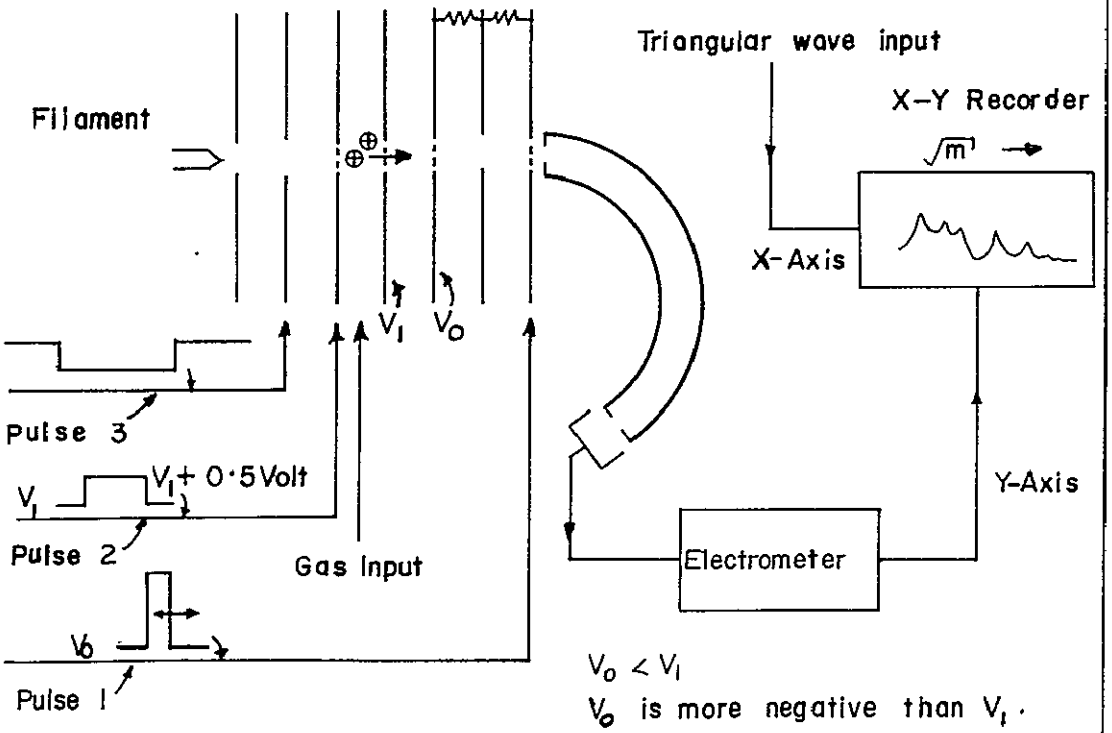

Fig.6.4.b: Block Diagram of Suggested Decelerating CMMA Mode II

this system and that of Figure 6.3a can be very high. Therefore, the sweeping rate of the pulse can be much higher than now, then with an improved electrometer (R. F. Reiter, 1976), one can get a reasonable resolution at very high sensitivity. This then would be suitable for a rocket experiment in the ionosphere.

In Figures 6.4a and 6.4b is shown another possible version of the decelerating mode constant-momentum mass spectrometer for residual gas analysis.

In Figure 6.4a, the electron beam applied to the ionization region is turned off as Pulse 3 is turned on, then a pulse is applied to the repeller plate in the ionization region as Pulse 2. If the duration of Pulse 2 is long enough, most of the ions will leave the ionization region before the electron beam is on again. The first end plate of the pulsing region is maintained at a more negative potential than the ionization region, and thus the ions acquire the required initial energy when they enter the pulsing region. After Pulse 2 is off, a decelerating pulse (Pulse 1) is applied to the last end plate of the pulsing region. The ions traversing the pulsing region are then analyzed by a sector field.

One can also achieve this result by putting the filament in line with the axis of the ionization region as well as the axis of the pulsing region (Figure 6.4b). Pulse 3 is used to switch off the electron beam. Then Pulse 2 is used to repel the ions from the ionization region into the pulsing region. The first end plate of the pulsing region is maintained at a more negative potential, V_o, than the potential in the ionization region, V_1; thus giving the ions their required initial energy. The decelerating pulse (Pulse 1) will

be on after Pulse 2 is off. Whatever ions were in the pulsing region before the electron beam was turned off will be repelled and only those ions from the ionization region will be analyzed.

Both cases in Figures 6.4a and 6.4b should give a higher sensitivity than the ones that we have now. Their resolution can be comparable or better than the ones that we have now. With a higher sensitivity, a fast sweeping rate can be used. Therefore these modes of operation will be suitable for rocket-borne experiments in the ionosphere.

Notice also that the estimation of flight path in all these suggested modes of operations can be as low as 5 to 6 cm. Therefore, they can be used up to a higher pressure (10^{-3} Torr for example).

REFERENCES

American Vacuum Society Standard, Journal of Vacuum Science and Technology, September, 1972.

Bracher, J., Ein Massenspektrometer hoher Empfindlichkeit, Zeit. Angew. Phys. 19, 345, 1965.

Brubaker, W. M., Mass spectrometer, U.S. Patent 2,157,985 filed June 5, 1958.

Brubaker, W. M., Simplified units and equations appropriate for use with mass spectrometer calculations, Proceedings of ASTM-E14 Conference, Dallas, Texas, May 1966, p. 528.

Dayton, I. E., J. M. Sarri and R. I. Schoen, A new type of low-resolution mass spectrometer, Boeing Scientific Laboratory's Report No. DI-82-0508, Clearinghouse for Federal Scientific and Technical Information, Report No. A.D. 634-235, 1966.

Dushman, S., Scientific Foundations of Vacuum Technique, John Wiley and Sons, Inc., 1949.

Fiks, V. B., Soviet Phys. (Doklady), 1, 89, 1956.

Hipple, J. A., Analysis by imparting unequal energies to ions, U.S. Patent 2,764,691, filed August 3, 1953.

Kanaya, K., H. Kawakatsu, H. Yamazaki and S. Sibata, Electron optical properties of three electrode electron lenses, Journal of Scientific Instruments, Vol. 43, 416, 1966.

Kendall, B. R. F., Bulletin of the Radio and Electrical Engineering Division, National Research Council of Canada, 9, No. 2, 22, 1959.

Kendall, B. R. F., Mass spectrometry, Bulletin of the Radio and Electrical Engineering Division, National Research Council of Canada, 10, No. 1, 25, 1960.

Kendall, B. R. F. and D. R. David, High-vacuum system for teaching and research, American Journal of Physics, 36, 234, 1968.

Kendall, B. R. F. and H. M. Luther, Apparatus for teaching and research in electron physics, American Journal of Physics, 34, 580, 1966.

Klemperer, O. and M. E. Barnett, Electron optics, Cambridge University Press, 1971.

Linear and interface circuits data book for design engineers, Texas Instruments, 1973.

Luther, H. M., Evaluation of the constant momentum mass spectrometer for ionospheric investigations, PSU-IRL-SCI-283, The Pennsylvania State University, 1966.

Luther, H. M., An investigation of mass dispersion in electric impulsive fields, PSU-IRL-SCI-349, The Pennsylvania State University, 1970.

Luther, H. M. and B. R. F. Kendall, Constant momentum mass spectrometer for ionospheric investigations, Proceedings of the ASTM-E14 Conference, Dallas, Texas, May, 1966, p. 369.

Miller, W. R. and N. Axelrod, Modified Faraday cage, Review of Scientific Instruments, 37, 1096, 1966.

Reiter, R. F., Rocket-Borne time-of-flight mass spectrometry, PSU-IRL-SCI-444, The Pennsylvania State University, 1976.

Spangenberg, K. R., Fundamentals of electron devices, McGraw-Hill Book Company, 1957.

Spencer, N. W., Upper atmospheric studies by mass spectrometry, Advances in mass spectrometry, Vol. 5, 1971, p. 509.

Steckelmacher, W., Energy analyzers for charged particle beams, Journal of Physics E: Scientific Instruments, 6, 1061, 1973.

Wolff, M. M. and W. E. Stephens, A pulsed mass spectrometer with time dispersion, Review of Scientific Instruments, 24, 616, 1953.